NUMBER _____ OF _____

# AUTHOR QUERIES

DATE 08/08/02
JOB NAME TMRI
JOB NUMBER 51415

ARTICLE 03x (MRI20301)
QUERIES FOR AUTHOR Morana et al.

**THIS QUERY FORM MUST BE RETURNED WITH ALL PROOFS FOR CORRECTIONS**

1) Kinetics meant?

2) Please define CTAP.

3) 555A?

4) 555A?

5) Please clarify the following sentence.

6) Word?

7) Expansion of HCV correct?

8) Please update in press reference.

9) Please supply year of publication.

10) Please verify name of publisher.

11) Please expand PD.

12) No legend for panels c and d?

NUMBER _____ OF _____

# PRODUCTION EDITOR QUERIES

DATE __08/08/02__
JOB NAME __TMRI__
JOB NUMBER __51415__

ARTICLE __03x (MRI20301)__
AUTHORS __Morana et al.__

**THIS QUERY FORM MUST BE RETURNED WITH ALL PROOFS FOR CORRECTIONS**

1) ED: Delete bracket?

2) ED: Should e be f?

*Topics in Magnetic Resonance Imaging*
**13**(3): 117–150


# Contrast Agents for Hepatic Magnetic Resonance Imaging

Giovanni Morana, M.D., Luigi Grazioli, M.D., Marco Testoni, M.D., Paolo Caccia, M.D., and Carlo Procacci, M.D.

**Summary:** The current availability of liver-specific contrast media (LSCM) allows the possibility to obtain an accurate diagnosis when studying focal liver lesions (FLL). It is necessary to have an in-depth knowledge of the biologic and histologic characteristics of FLL and the enhancement mechanism of LSCM to gain significant accuracy in the differential diagnosis of FLL. It is possible to subdivide FLL into three main groups according to the cinetic of contrast enhancement: hypervascular FLL, hypovascular FLL, and FLL with delayed enhancement. Dynamic contrast-enhanced magnetic resonance imaging is an important tool in the identification and characterization of FLL. LSCM with a first phase of extracellular distribution give both dynamic (morphologic) and late phase (functional) information useful for lesion characterization. With LSCM it is possible to differentiate with high accuracy benign from malignant lesions and hepatocellular from nonhepatocellular lesions. To understand contrast behavior after injection of LSCM, it is necessary to correlate contrast enhancement with the biologic and histologic findings of FLL. **Key Words:** Liver—Neoplasms—Magnetic resonance—Contrast media.

AU1

## INTRODUCTION

Magnetic resonance imaging (MRI) is an established imaging method for evaluation of focal liver lesions, although the accuracy of unenhanced MRI for lesion characterization is comparatively low (1,2). To adequately characterize focal hepatic lesions on MRI, it is necessary to use contrast media (CM) that are able to modify the signal intensity of either the lesion or the normal liver parenchyma and thus contribute to characterization of the lesion (3–6).

The sensitivity of MR to the variations of signal intensity induced by CM has led to the development of several different types of CM, which use the paramagnetic properties of gadolinium (Gd) or manganese or the superparamagnetic properties of iron. The various CM can be distinguished on the basis of their distribution after intravenous injection.

From the Radiological Department, University of Verona, Verona, Italy (G.M., M.T., C.P.); and the Radiological Department, University of Brescia, Brescia, Italy (L.G., P.C.).

Address correspondence and reprint requests to Dr. Giovanni Morana, Radiological Department, Policlinico G.B. Rossi,

Piazzale L.A. Scuro 10. 37134 Verona, Italy, or giannimorana@interfree.it

## OVERVIEW OF CONTRAST AGENTS

Nonspecific Gd chelates such as Gd-DTPA (Magnevist, Schering AG, Berlin, Germany) and Gd-DTPA-BMA (Amersham Health, Oslo, Norway) (7) that distribute in the extracellular fluid (ECF) space currently are the most widely used CM. These CM are most effective during the dynamic phase of contrast enhancement when differential blood flow between tumor and normal liver parenchyma leads to characteristic lesion enhancement patterns (4,5). Unfortunately, dynamic phase imaging alone can, at times, prove unsatisfactory for the accurate diagnosis of hepatic lesions (1).

The development of CM with liver-specific properties has increased the accuracy of MR for the identification and characterization of focal liver lesions (8–11).

Exclusive distribution to the *hepatocellular compartment* can be obtained using CM that–when injected by slow infusion–accumulate within the hepatocytes and cause an increase in the proton relaxation rate. In mangafodipir trisodium (Mn-DPDP, Teslascan, Nycomed, Oslo, Norway), the manganese ion is chelated with four molecules of meglumine. The molecule is isotonic with the blood and has a low viscosity. In Europe it is infused


DOI: 10.1097/01.RMR.0000027140.44506.4E

slowly (2 to 3 mL/min over 10 to 20 minutes) at a concentration of 10 mmol/mL and at a dose of 0.5 mL/kg. In the United States, a faster injection (about 1 minute) is used. The need for slow infusion of Mn-DPDP and the ensuing lack of a dynamic imaging capability has led some authors to propose the possibility of sequential administration of Gd chelates and Mn-DPDP in a single visit to obtain both dynamic and late imaging (12).

After administration, the $Mn^{2+}$ ion contained in the molecule is gradually released into the blood from the DPDP chelate and is substituted by zinc. The latter has an affinity for the chelant that is hundreds of times greater than that of $Mn^{2+}$. The free $Mn^{2+}$ then is available for uptake into parenchymal cells, particularly those of the liver, pancreas, kidneys, and adrenals in which metabolism of this metal takes place. The maximum tissue enhancement is observed at the end of the infusion after approximately 20 minutes and lasts for about 4 hours (13). The liver parenchyma enhances significantly after Mn-DPDP administration. Tumors of nonhepatocytic origin show little or no tumor enhancement, resulting in increased lesion conspicuity. Several studies have shown improved lesion detection on images obtained after infusion of Mn-DPDP compared with precontrast images (14,15). However, uptake of $Mn^{2+}$ after Mn-DPDP infusion has been observed in hepatic metastases from nonfunctioning endocrine tumors of the pancreas (16).

Many hepatocellular lesions, on the other hand, show mass enhancement, thereby resulting in decreased tumor liver contrast/noise ratio (CNR). An investigation aimed at evaluating Mn-DPDP for the study of hepatocellular carcinoma (HCC) demonstrated poor efficacy of this agent for the identification of these lesions (17).

In a recent multicenter study, Mn-DPDP–enhanced MRI in 77 patients with histologically confirmed lesions had a sensitivity and specificity in differentiating lesions of 91% and 67% (malignant versus benign lesions) and 91% and 85% (hepatocellular versus nonhepatocellular lesions), respectively (18). Uptake of Mn-DPDP, and therefore enhancement, by both benign and malignant hepatic neoplasms limits the accurate differentiation between benign and malignant tumors of hepatocellular nature (17–20) and represents a major shortcoming of this agent.

Other CM demonstrate *combined perfusion and hepatocyte-selective properties*. Such compounds distribute initially to the vascular-interstitial compartment in a manner analogous to that of conventional extracellular CM. Thereafter, a fraction of the injected dose is taken up into the hepatocytes, causing an increase of the signal intensity of the hepatic tissue. Agents of this type include gadobenate dimeglumine (Gd-BOPTA), which is approved in Europe for clinical use, and gadolinium-ethoxybenzyl-diethylenetriaminepentaacetic acid (Gd-EOB-DTPA), which is in an advanced phase of development.

*Gadobenate dimeglumine* (Gd-BOPTA, MultiHance, Bracco Imaging S.p.A., Milan, Italy) is a chelate of the paramagnetic Gd ion, salified with two molecules of meglumine. Gd-BOPTA is a second-generation Gd chelate that combines the properties of a conventional extracellular Gd agent with those of an agent targeted specifically to the liver (21).

Two features that distinguish Gd-BOPTA from the conventional Gd chelates are a capacity for weak and transient interaction with serum albumin (22) and an elimination profile in which approximately 96% of the injected dose is excreted renally via glomerular filtration; the remaining 2% to 4% taken up by functioning hepatocytes is eliminated in the bile via the hepatobiliary pathway (23). Whereas the former feature confers on Gd-BOPTA a twofold greater T1 relaxation rate in vivo, the latter leads to a marked and long-lasting enhancement of the signal intensity of normal liver parenchyma, resulting in an additional delayed imaging window beginning 40 minutes after Gd-BOPTA administration (24).

Studies have shown that although Gd-BOPTA behaves in a manner analogous to conventional Gd agents during the dynamic phase of contrast enhancement (25), in the delayed phase it not only improves the impact of MRI for the detection of focal liver lesions (3,26) but it also may contribute to the improved characterization of detected lesions, particularly lesions demonstrating atypical enhancement on dynamic imaging (27,28).

*Gadolinium ethoxybenzyl-diethylenetriaminepentaacetic acid* (Gd-EOB-DTPA, Schering AG) exploits the "carrier" used by hepatocytes for the uptake of bilirubin (29). In a manner analogous to that of Gd-BOPTA, this CM distributes initially to the vascular-interstitial compartment after injection. However, whereas only 2% to 4% of the injected dose of Gd-BOPTA is taken up by hepatocytes and eliminated in the bile, in the case of Gd-EOB-DTPA approximately 50% of the injected dose is taken up and eliminated via the hepatobiliary pathway after approximately 60 minutes. The maximum increase of liver parenchyma signal intensity is observed approximately 20 minutes after injection and lasts for approximately 2 hours (30). During the perfusion phase, the dynamic enhancement patterns seen after injection of Gd-EOB-DTPA are similar to those seen with Gd-DTPA, whereas during the hepatobiliary phase Gd-EOB-DTPA–enhanced images have been shown to yield a statistically significant improvement in the detection rate of metastases, HCCs, and hemangiomas compared with unenhanced and Gd-DTPA–enhanced images (11).

Use of the superparamagnetic effect of iron oxide particles is based on a *distribution in the reticuloendothelial system* (RES). Superparamagnetic CM consist of iron oxide particles, coated with a polysaccharide, whose paramagnetic ions produce domains of spontaneous magnetization that align their magnetic dipole moments with and become strongly magnetized by an external magnetic field (31,32). The presence of superparamagnetic iron oxide (SPIO) locally augments the externally applied magnetic field, producing magnetic field heterogeneity that, in turn, promotes dephasing and results in signal loss from enhanced T2 relaxation. SPIO particles are cleared from the blood by phagocytosis accomplished by RES, usually lacking in most malignant liver lesions, so that uptake is observed in the normal liver, spleen, bone marrow, and lymph nodes (33). Inflammation, scarring, regeneration, and shunting in cirrhotic liver reduces hepatic uptake of SPIO, shifts distribution to the spleen, and produces signal heterogeneity.

Cirrhotic liver tissue can show an inhomogeneous decrease of liver signal intensity, representing collagenous structures. Nevertheless, Yamashita et al. (34) observed that the uptake of SPIO did not correlate with chronic liver parenchymal pathology, indicating that Kupffer cells activity does not correlate with progress of periportal fibrosis, although reductions in signal intensity were small in severely cirrhotic liver. This is probably because the functional status of Kupffer cells is closely correlated with hepatic function rather than the degree of fibrosis, suggesting that a larger amount of SPIO might be required to obtain sufficient contrast in patients with poor liver function.

Most focal liver lesions, mainly those that are malignant, lack Kupffer cells or the capacity to take up particles. After SPIO injection the darkening of normal liver parenchyma that surrounds focal liver lesions increases the CNR of these lesions, usually slightly hyperintense on precontrast T2-weighted images, which appear more hyperintense on T2-weighted images.

The T1 relaxivity of SPIO is a function of the surface area, because it requires intimate contact between water molecules and the surfaces of the iron oxides. It increases when the particles are dispersed in the solvent and no longer concentrated in a small volume. Therefore, a T1 effect predominates at low concentrations. SPIO particles are taken up by Kupffer cells and concentrated in lysosomes in the form of a cluster. In this configuration the small particles behave like large inhomogeneously distributed ferrite particles and distort the local magnetic field. For this reason T2* is significantly shortened and obscures any effect, even on T1-weighted images (35).

Several studies have attempted to determine the optimal pulse sequence for post-SPIO imaging of hepatic lesions. Pulse sequences that are sensitive to magnetic field heterogeneity tend to be sensitive to the presence of iron oxide. T2*-weighted gradient-echo images are sensitive to SPIO (36), whereas T2-weighted spin-echo images are more sensitive than T2-weighted fast spin echo, as the multiple rephasing pulses used in the latter tend to obscure signal losses arising from local variations in the magnetic environment (37). Echo-planar images are sensitive to SPIO (38).

In a recent study, Alger et al. (39) found that CNR differences attributable to TE variation over the range from 46 to 106 milliseconds were less than 34% for a 0.2-T unit, and TE of 46 milliseconds yielded a statistically significantly greater CNR than did TE of 76 or 106 milliseconds. The same was true at the higher field strength, but differences were not significant. The authors also found that post-SPIO CNR was significantly greater at 1.5 T than at 0.2 T. Moreover, in the specific case of post-SPIO liver imaging there is no agreement in the evaluation of string field influence. Deckers et al. (40) found no significant CNR differences between 0.2 and 1.5 T, whereas Alger et al. (39) found the opposite.

A variety of iron oxides have been developed for CM-enhanced MRI. Two different classes of iron oxides are commercially available or in phase III clinical trials: superparamagnetic ferumoxides (SPIO) and ultrasmall superparamagnetic iron oxides (USPIO).

*Ferumoxides* (Feridex IV, Berlex Laboratories Wayne, NY, USA; and Endorem, Guerbet, Aulnay Sous Bois, France) was developed by Advanced Magnetics (Cambridge, MA, USA) and is referred to as AMI-25. It has been commercially available in Europe since 1995 and was introduced to the U.S. market in 1996. Ferumoxides is an SPIO colloid with low-molecular-weight dextran, with a particle size of 50 to 180 nm according to the analytical system used (electron microscopy or photo correlation spectroscopy) (41).

About 8 minutes after intravenous injection, iron oxide particles are taken up by the reticuloendothelial cells in the liver (Kupffer cells) and in the spleen, with approximate uptake of 80% and 6% to 10%, respectively (33). Maximum signal loss is obtained after 1 hour, with an imaging window ranging from 30 minutes to 6 hours after injection (42,43). Most studies in the United States and Japan used a dose of 10 mmol/kg, whereas the recommended dose in Europe has been 15 mmol/kg. To reduce the incidence of side effects such as hypotension, ferumoxides is prepared as a dilution in 100 mL of 5% dextrose and administered as a drip infusion over 30 minutes. Hypotension and lumbar pain represent the most frequent symptoms associated

with SPIO administration, with an incidence ranging from 2% to 10% (41).

Clinical efficacy of ferumoxides for detection focal liver lesions on T2-weighted images has been investigated in several trials, most of which supported the value of postcontrast images for detection of solid liver lesions. In a multicenter trial, ferumoxides-enhanced T2-weighted images revealed additional lesions not seen on unenhanced images in 27% of cases and additional lesions not seen by conventional (nonspiral) computed tomographic (CT) scans in 40%. The additional information would have changed therapy in 59% (43). A comparison with spiral CT demonstrated a better sensitivity of SPIO-enhanced MR images but at the expense of reduced specificity with a higher number of false-positive results (44). Other studies comparing the efficacy of SPIO-enhanced AU2 T2-weighted MRI with CTAP showed higher sensitivity and specificity of MRI, especially with T2*-weighted breath-hold gradient-recalled echo (GRE) images. Those images were effective in distinguishing metastases from small cysts, a source of false-positive results for CTAP (45). A previous study demonstrated a better sensitivity of CTAP when performed with spiral CT (46).

*SHU 555 A* (Ferucarbotran) is the code name of an SPIO contrast agent registered as Resovist (Schering AG). It has been commercially available in some European countries since 2001. The active particles are carboxydextran-coated superparamagnetic iron oxide, with a hydrodynamic diameter ranging from 45 to 60 nm. The different particle sizes determine the velocity of their uptake by cells of the RES, especially the Kupffer cells in the liver, as well as the relaxivity-related effects. SHU 555 A exhibits a low viscosity and is isotonic to blood plasma. It is the first liver-specific contrast agent for MRI consisting of SPIO particles that can be administered as a fast bolus.

SHU 555 A has a strong effect on the shortening of T1 and T2 relaxation times. R1 and R2 relaxivities in blood (at 1.5 T and 37°C) are 7.2 ± 0.1 and 82.0 ± 6.2 L/(mmol × sec), respectively. Because of the high R2 relaxivity it is particularly suited to T2-weighted and T2*-weighted imaging. Furthermore, SHU 555 A enables T1-weighted imaging with one tenth the standard dose of extracellular contrast agents (Gd-DTPA), ensuring a valuable although less pronounced T1 effect. Fast bolus injection of SHU 555 A makes possible observation of the early perfusion characteristics of the liver using T1-weighted or T2*-weighted sequences.

There are some interesting perspectives with regard to dynamic imaging with SPIO enhancement that can be ad- AU3 dressed with SHU 555. With rapid imaging during injection of SHU 555 A, while the particles are still in the circulation, signal enhancement from intrahepatic vessels can be seen on T1-weighted images. The designation of vessels during this phase can provide a reference for interpretation on delayed T2-weighted images. This presents an opportunity to circumvent a previously reported limitation of SPIO agents, i.e., the differentiation of the bright signal intensity of small liver lesions from the bright signal intensity of blood vessels viewed in cross section may be a challenge on delayed SPIO-enhanced MR images (47).

During the perfusion phase the T1 effects of SPIO can be exploited to assist in the diagnosis of hemangiomas (48), a property that also is relevant to SHU55A (49). Accumulation phase imaging (RES phase) can be performed as early as 10 minutes after injection using T1-weighted, T2-weighted, and T2*-weighted sequences. T2-weighted and T2*-weighted accumulation phase imaging improves the visualization, delineation, and conspicuity of lesions and hence improves detection (50). However, the combined approach of nonenhanced and SPIO-enhanced T2-weighted MRI together resulted in a significantly higher sensitivity and significantly more accurate differentiation of benign from malignant lesions compared with results from spiral CT images, nonenhanced T2-weighted MRI, or SPIO-enhanced T2-weighted images alone (51).

*AMI-227* (Advanced Magnetics) belongs to the USPIO class of iron oxide compounds. AMI-227 is known by different code names during clinical trials. It consists of a 5-nm–diameter iron oxide core coated with low-molecular-weight dextran, yielding a particle with a mean diameter of 17 to 20 nm. The smaller particle size results in a long intravascular half-life of more than 200 minutes; thus, AMI-227 is considered a blood pool agent (52). The uptake of AMI-227 in the RES system is more delayed compared with SPIO, and there is greater bone marrow and lymph node uptake than occurs with larger SPIO (41).

As is typical of iron oxide contrast agents, AMI-227 shows preferential or selective accumulation in the liver parenchyma, resulting in signal loss in the liver on T2-weighted images. Most solid liver tumors, particularly metastases, which lack phagocytic activity, do not show significant signal intensity decrease, resulting in augmented CNR between liver and metastases.

On T1-weighted images there is signal enhancement in the distribution site of the USPIO, including liver tissue, blood, and hemangiomas. After AMI-227 administration hemangiomas are bright on T1-weighted images and lose signal on T2-weighted images. This is different from metastases, which remained unchanged on T1-weighted and T2-weighted postcontrast images (53). In that study, about 87% of all hemangiomas demonstrated uniform hyperintensity on T1-weighted postcontrast images. Conversely, HCC and hypervascular metastases lacked uniform hyper-

intensity on T1-weighted images after administration of USPIO. This difference in T1 enhancement characteristics, in association with the characteristic drop in signal intensity for hemangiomas on T2-weighted postcontrast images, facilitated high sensitivity and specificity values in the characterization of these lesions.

Demonstration of ring enhancement after USPIO has been proposed as a means to differentiate benign from malignant liver lesions. With USPIO, it has been suggested that this rim enhancement may be due to blood pool enhancement in peripheral vessels surrounding malignant tissue (54). In one report, hemangioma rarely demonstrated ring enhancement, whereas metastases showed ring enhancement in about 30% of the cases, providing a helpful sign to differentiate hemangiomas from malignant liver lesions (53).

## BEHAVIOR OF FOCAL LESIONS IN RESPONSE TO CONTRAST MEDIA

A practical approach to focal hepatic lesions involves classifying the behavior of lesions on dynamic imaging with contrast media that distributes in the ECF spaces, so-called ECF agents. This is the most frequently used method for characterization of focal hepatic lesions relied upon for both MRI and CT. This approach yields methods to facilitate the detection and characterization of lesions, the latter relying upon recognition of distinctive patterns of enhancement.

The *hypervascular liver lesions* consist of a wide range of lesion types, ranging from physiopathologic to pathologic. Among these lesion types are benign and malignant lesions of both hepatocellular and nonhepatocellular origin.

The discussion of hypervascular lesions begins with benign focal masses derived from hepatocellular origins.

### Benign focal masses derived from hepatocellular origins

*Focal nodular hyperplasia* (FNH) is the second most common benign lesion of the liver behind hemangioma. It is present in 3% to 5% of the population and is more common in women of child-bearing age (55). The cellular structure of FNH is similar to that of normal hepatic parenchyma apart from the presence of an abnormal biliary system. FNH is a benign tumor-like lesion that results from a hyperplastic rather than a neoplastic process (56).

In more than one third of cases the lesion develops asymptomatically and is discovered incidentally. In other cases there may be some signs or symptoms indicative of its presence. In roughly 85% of cases only a single nodule of FNH is present. The margins of the lesion usually are well defined, and its size is generally smaller than 5 cm, although lesions between 8 and 10 cm can be encountered (57). Given the low risk of rupture and hemorrhage and the low level of malignancy, FNH frequently is left untreated but with regular follow-up examinations, particularly of asymptomatic cases (58).

On T1-weighted MRI, FNH appears isointense or slightly hypointense to the surrounding liver parenchyma and may show a central hypointense scar. On T2-weighted images the lesion is slightly hyperintense. Contrast-enhanced dynamic phase MRI using traditional ECF Gd-based contrast agents gives similar dynamic information as CT and provides the greatest diagnostic sensitivity among the techniques in current use. This is the case when dynamic MR data are combined with the information available on unenhanced T1-weighted and T2-weighted images (59).

Dynamic MRI shows a marked enhancement in the arterial phase of the lesion, which persists as slightly hyperintense or isointense in the portal venous and distribution phase (Figs. 1 and 2), whereas the central scar appears F1,F2 hypointense in the arterial and portal venous phase to become hyperintense in the distribution phase (Fig. 2e).

Accurate characterization of FNH is not always possible because atypical features can confound the interpretation. In a recent study the majority (86%) of small (3 cm or less) FNH did not have a visible scar on unenhanced or enhanced dynamic phase scans (28). Other investigators reported similar findings on MR and CT (60–62). Although the absence of a scar in small FNH cannot be considered "atypical," it makes it more difficult to distinguish FNH from other hypervascular neoplasms.

MR contrast agents with liver-specific properties are helpful in characterizing FNH. In FNH, there is prolonged and excessive hepatocellular accumulation of hepatocytic-specific CM due to the structural alteration of the biliary-canalicular system that does not communicate with or derive from the surrounding normal hepatic biliary system (63).

Gd-BOPTA offers the possibility of dynamic imaging and evaluation of delayed phase images. The Gd-BOPTA enhancement dynamics of FNH in the early phases parallel those seen with ECF agents. On T1-weigted images substantial enhancement is noted within the parenchyma of the lesion, whereas the central scar, which is the principal site of the biliary metaplasia, appears consistently hypointense in the delayed phase. The lesion appears isointense or hyperintense to the surrounding liver, with three different patterns of enhancement frequently observed: homogeneous (Fig. 1e), peripheral (Fig. 2f), or heterogeneous (Fig. 3e) (28). Similar findings have been F3 observed with Mn-DPDP (Fig. 1f) (19).

Kupffer cells usually are observed within FNH and,

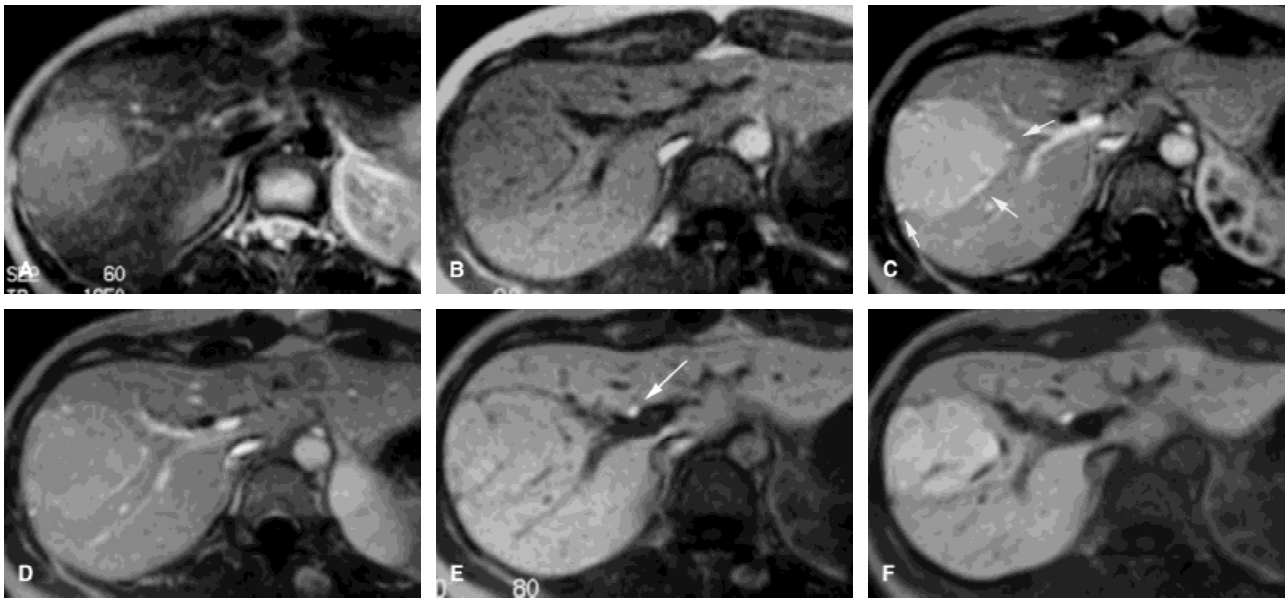


**FIG. 1.** Atypical focal nodular hyperplasia in 34-year-old woman with chronic right upper abdominal pain. **a:** SE transverse T2-weighted image shows a large homogeneous slightly hyperintense lesion in the right lobe of the liver, without any evidence of central scar. **b:** GRE transverse T1 precontrast image. The lesion is homogeneously isointense to the surrounding liver parenchyma. During dynamic imaging (GRE transverse T1-weighted), the lesion is homogeneously hyperintense at arterial phase. **c:** At 25 seconds after bolus administration of Gd-BOPTA, large peripheral feeding vessels are evident (arrows). **d:** In the portal venous phase obtained 90 seconds after the injection, the lesion persists as slightly hyperintense, but there is no evidence of scar. **e:** GRE transverse T1-weighted images obtained 2 hours after administration of Gd-BOPTA. There is homogeneous enhancement of the liver, and the lesion appears homogeneously isointense. The main biliary duct is hyperintense due to biliary elimination of Gd-BOPTA (arrow). **f:** Follow-up after 1 year. GRE transverse T1-weighted images obtained 1 hour after administration of Mn-DPDP. There is homogeneous enhancement of the liver, and the lesion appears markedly hyperintense. No scar is appreciable. With this contrast media the main biliary duct is hyperintense because of biliary elimination.

along with malformed bilary ducts, are a major histologic feature of this lesion. Uptake of SPIO by FNH is common, with the lesions showing significant decreases in signal intensity on ferumoxides-enhanced T2-weighted images (64). Signal drop reflects the presence of Kupffer cells within the lesion.

Nevertheless the amount and distribution of Kupffer cells within the nodule can vary and yield different patterns of signal decrease: some small FNH (less than 3 cm) show homogeneous signal drop similar to that observed in the surrounding parenchyma, whereas large FNH may show heterogeneous signal drop (Fig. 3g). The central scar excludes iron particles and is readily demonstrated as hyperintense central stellate area. That finding corresponds to the high signal area seen on T2-weighted precontrast images but higher conspicuity generally is found after the use SPIO agents (Fig. 2g) (65).

In a comparison of 33 patients with 55 FNH studied with Gd-BOPTA and with SPIO (Endorem), 16 (29%) of 55 smaller lesions were not visible on T2-weighted images both before and after SPIO, whereas all lesions were visible on dynamic phase imaging with Gd-BOPTA. Overall, typical behavior was observed for 52 (94.5%) of 55 lesions after Gd-BOPTA and for 24 (61.5%) of 39 visible lesions after Endorem. MRI with Gd-BOPTA was superior to MRI with Endorem for the identification and characterization of FNH (100% versus 71% and 94.5% versus 61.5%, respectively) (66).

*Nodular regenerative hyperplasia* (NRH) of the liver is not a specific entity but is a secondary and nonspecific tissue adaptation to heterogeneous distribution of blood flow, characterized by multiple monoacinar regenerative nodules in the absence of fibrous septa. These lesions can be imaged when the nodules become confluent. NRH occurs in 5.6% of individuals older than 80 years and with increased frequency in patients with systemic arthritis, polymyalgia rheumatica, massive tumor infiltration, and mineral oil deposition (67). Clinically NRH presents primarily with manifestations of noncirrhotic portal hypertension in about 50% of the patients. Management is directed primarily to portal hypertension and variceal bleeding, which is the main source of mortality. Liver failure is uncommon because of satisfactory preservation of liver function (68). Malignant transformation of the nodules has never been reported.

On unenhanced MRI, NRH is isointense to hypointense on T2-weighted images and hyperintense to isointense on T2-weighted images. On contrast-enhanced dynamic phase MRI with extracellularly distributed CM, the lesion appears hyperintense during the arterial phase and isoin-

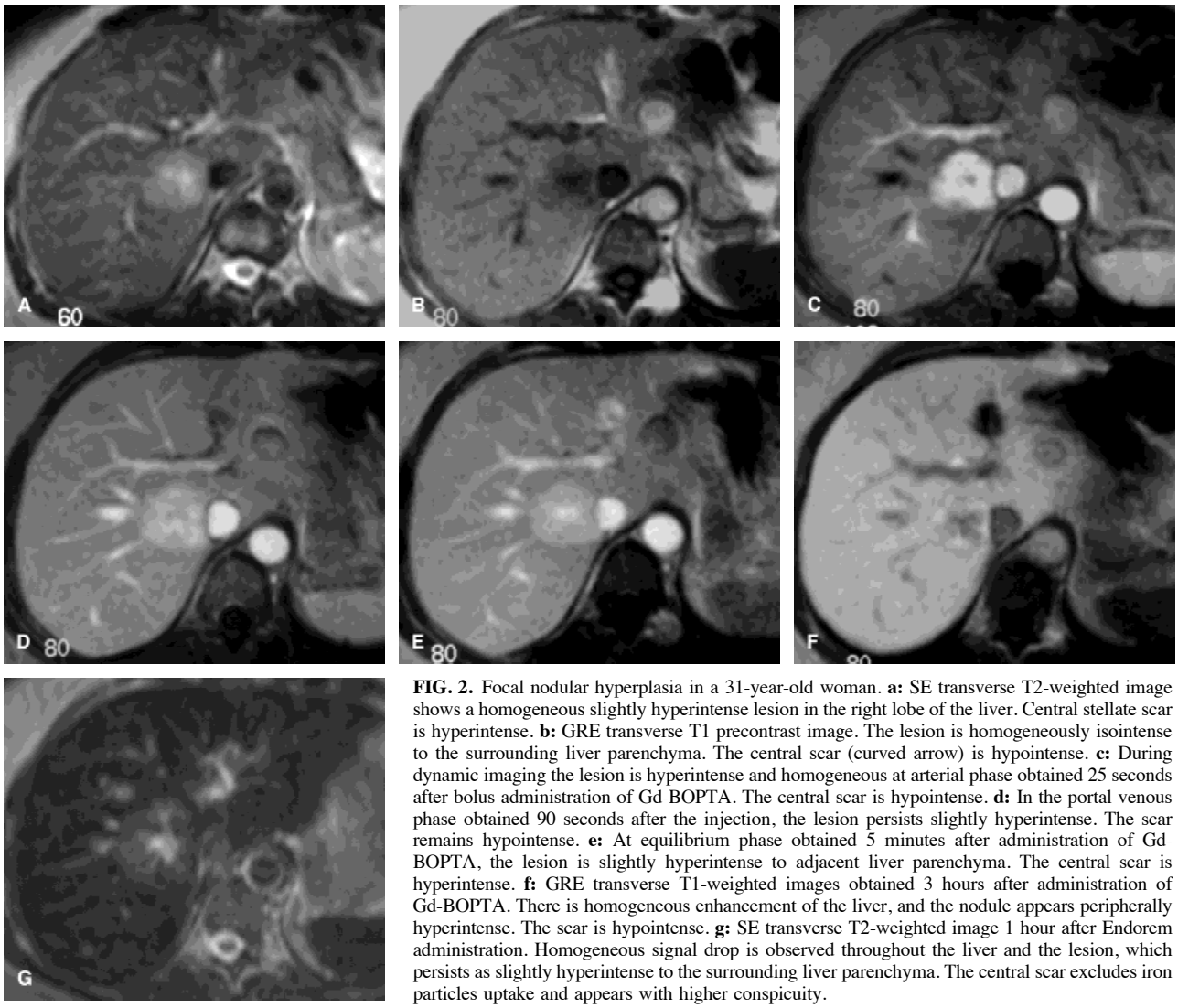


**FIG. 2.** Focal nodular hyperplasia in a 31-year-old woman. **a:** SE transverse T2-weighted image shows a homogeneous slightly hyperintense lesion in the right lobe of the liver. Central stellate scar is hyperintense. **b:** GRE transverse T1 precontrast image. The lesion is homogeneously isointense to the surrounding liver parenchyma. The central scar (curved arrow) is hypointense. **c:** During dynamic imaging the lesion is hyperintense and homogeneous at arterial phase obtained 25 seconds after bolus administration of Gd-BOPTA. The central scar is hypointense. **d:** In the portal venous phase obtained 90 seconds after the injection, the lesion persists slightly hyperintense. The scar remains hypointense. **e:** At equilibrium phase obtained 5 minutes after administration of Gd-BOPTA, the lesion is slightly hyperintense to adjacent liver parenchyma. The central scar is hyperintense. **f:** GRE transverse T1-weighted images obtained 3 hours after administration of Gd-BOPTA. There is homogeneous enhancement of the liver, and the nodule appears peripherally hyperintense. The scar is hypointense. **g:** SE transverse T2-weighted image 1 hour after Endorem administration. Homogeneous signal drop is observed throughout the liver and the lesion, which persists as slightly hyperintense to the surrounding liver parenchyma. The central scar excludes iron particles uptake and appears with higher conspicuity.

tense or slightly hyperintense in the portal and equilibrium phases (Fig. 4e and f) (69,70). Both with Gd-BOPTA and Mn-DPDP the lesion appear isointense or hyperintense to the surrounding liver parenchyma in the hepatobiliary phase (Fig. 4g and h). The appearance of NRH with SPIO CM has not yet been described, but because of the histologic characteristics of NRH its behavior is expected to be similar to that observed for FNH.

*Hepatic adenoma* (HA) is a benign neoplasm that typically is found in women with a history of oral contraceptive use (71,72). It is also seen in patients with type I glycogen storage disease (73). In these subjects, the HAs are likely to be multiple and more often undergo malignant transformation, although the latter still is considered rare (74). Other predisposing conditions, such as iron overload, have been described (75).

HA consist of plates or cords of cells that are larger than normal hepatocytes and contain large amounts of glycogen and lipid. Lipid accumulation is responsible for the characteristic yellow appearance of the cut surface of adenomas at pathology, and evidence of lipid at CT or MRI can be suggestive in diagnosing hepatocellular adenoma. The plates are separated by dilated sinusoids, which are thin-walled capillaries perfused by arterial pressure, but a portal venous supply is lacking. A tumor capsule usually is absent or incomplete. Kupffer cells often are found in HA but in reduced numbers and with little or no function, as reflected by the absent or diminished uptake of technetium (Tc)-99m sulfur colloid (76). Even though HA have functioning hepatocytes, they lack bile ducts, a key histologic feature that helps distinguish HA from FNH (63). It is likely that bilirubin metabolism is blocked

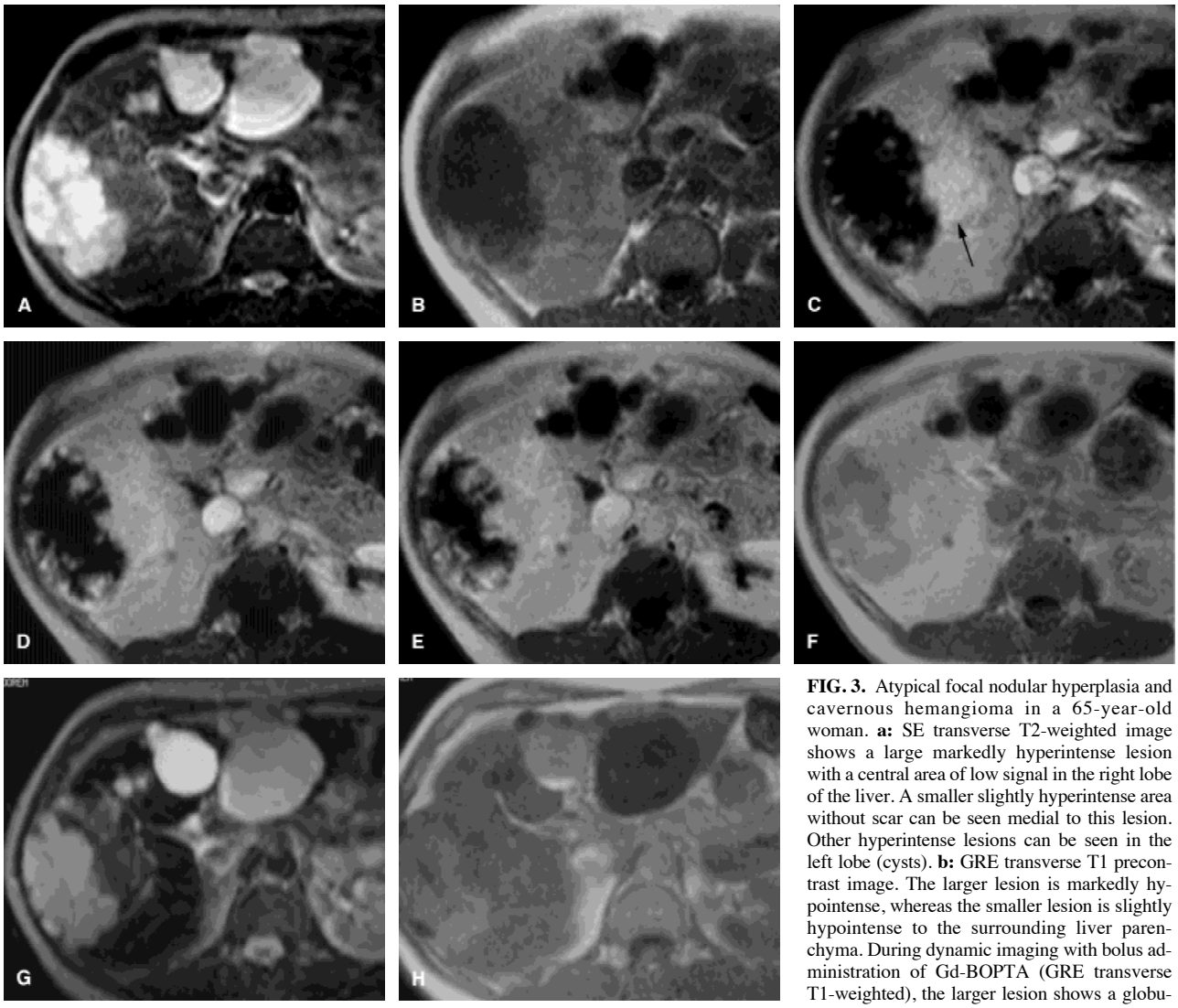


**FIG. 3.** Atypical focal nodular hyperplasia and cavernous hemangioma in a 65-year-old woman. **a:** SE transverse T2-weighted image shows a large markedly hyperintense lesion with a central area of low signal in the right lobe of the liver. A smaller slightly hyperintense area without scar can be seen medial to this lesion. Other hyperintense lesions can be seen in the left lobe (cysts). **b:** GRE transverse T1 precontrast image. The larger lesion is markedly hypointense, whereas the smaller lesion is slightly hypointense to the surrounding liver parenchyma. During dynamic imaging with bolus administration of Gd-BOPTA (GRE transverse T1-weighted), the larger lesion shows a globular peripheral enhancement, whereas the smaller lesion is homogeneously hyperintense at arterial phase (25 seconds after bolus administration) **(c),** to become slightly hyperintense in the portal venous phase (90 seconds after the injection) **(d),** and isointense at the distribution phase (3 minutes after the injection) **(e).** There is no evidence of scar. **f:** GRE transverse T1-weighted images obtained 1 hour after administration of Gd-BOPTA. There is homogeneous enhancement of the liver, and the larger lesion appears hypointense with the central fibrotic area slightly hyperintense due to pooling of CM. The smaller lesion appears inhomogeneously isointense. **(g,h)** Follow-up at 18 months, 1 hour after administration of Endorem. **g:** SE transverse T2-weighted images. Homogeneous signal drop is observed throughout the liver and the larger lesion, which persists slightly hyperintense to the surrounding liver parenchyma. The smaller lesion shows inhomogeneous uptake of SPIO; thus, it appears slightly more hyperintense than in the unenhanced study. **h:** GRE transverse T1-weighted image. The hemangioma appears hyperintense with the exception of the central fibrotic area. The focal nodular hyperplasia is isointense.

within the HA, as confirmed by the absence of bile within resected HAs (77).

Most patients are asymptomatic with normal liver function. Large HA may cause a sensation of right upper quadrant fullness or discomfort. The classic clinical manifestation of HA is spontaneous rupture or hemorrhage, especially for large and multiple adenomas, leading to acute abdominal pain and possibly progressing to hypotension or even death (77). Thus, there is a clinical indication for the surgical removal of large (greater than 5 cm) HA.

At MRI, HAs have a wide variety of appearances and have been variously described as hyperintense, isointense, and hypointense lesions (5,78,79). Areas of increased signal intensity on T1-weighted MRI can result from fat (35%–77%) and hemorrhage (52%–93%) (80–82), whereas low signal intensity areas correspond to necrosis, old hemorrhage, or calcifications (80). Some 47% to 74%

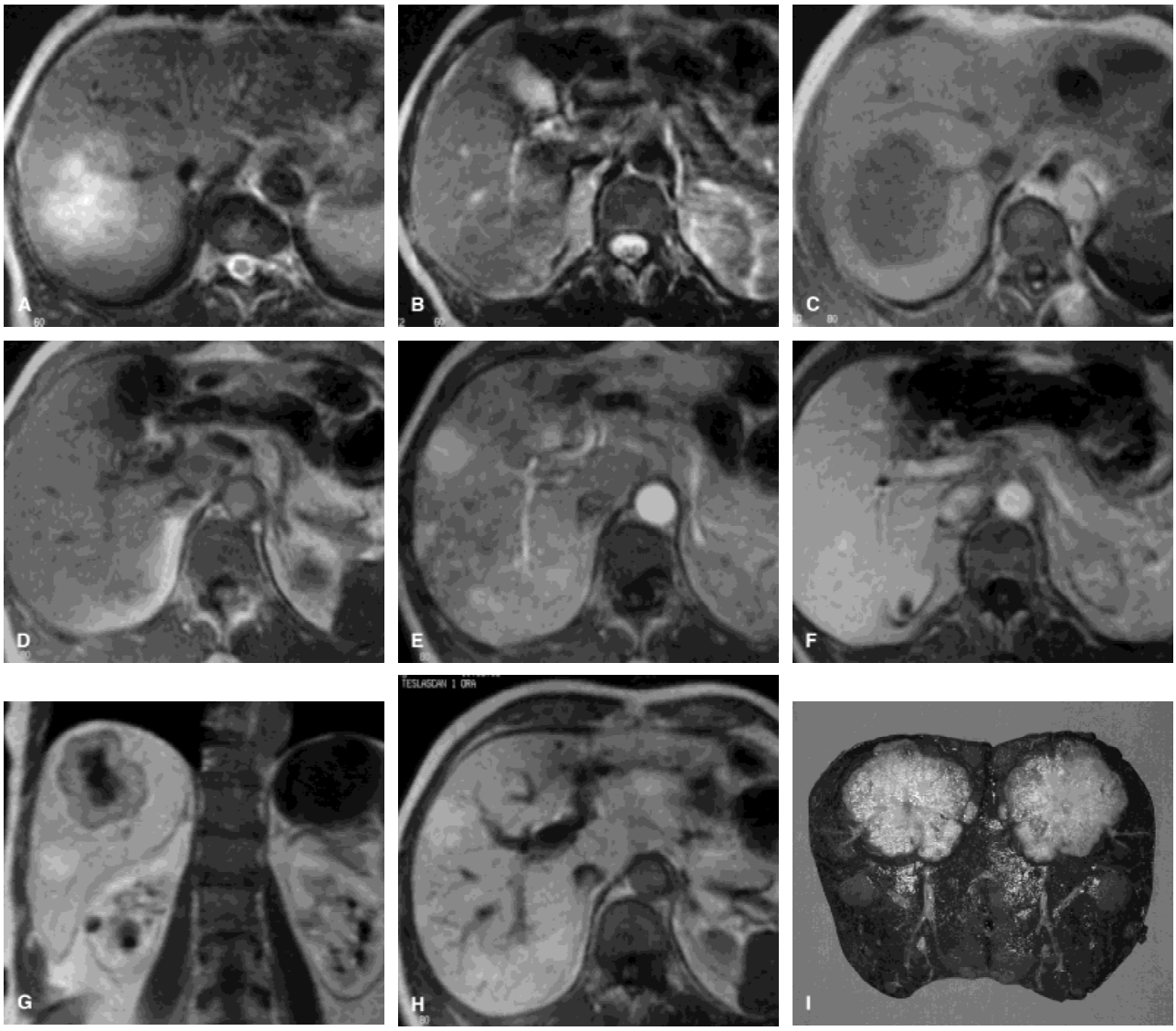


**FIG. 4.** Nodular regenerative hyperplasia in a 65-year-old man with a large peripheral cholangiocarcinoma. **a:** Nonenhanced T2-weighted SE transverse image shows a large hyperintense mass in the right lobe. **b:** At another level the T2-weighted SE sequence shows no lesions. **c:** On precontrast T1-weighted GRE image at the same level shown in panel a, the mass is hypointense compared with the parenchyma. **d:** PrecontrastT1-weighted images showed no lesions at the same level shown in panel b. Images obtained at the levels shown in panels b and d during dynamic imaging with Gd-BOPTA (GRE transverse T1-weighted) show multiple hypervascular lesions in the arterial phase **(e),** which appear isointense in the portal venous phase **(f).** Images obtained in the hepatobiliary phase, 1 hour after Gd-BOPTA injection, show that the large lesion is hypointense centrally on T1-weighted GRE coronal image with some peripheral enhancement **(g),** whereas other lesions appear isointense or hyperintense. **h:** On T1-weighted GRE transverse image 1 hour after Mn-DPDP, the same behavior is observed, with the lesions from the levels shown in panels b and d being isointense or hyperintense. **i:** In the surgical specimen the large cholangiocarcinoma shows a radiate aspect with a central fibrotic area, whereas the multiple nodules of nodular regenerative hyperplasia appear more similar to normal liver.

of HAs are predominantly hyperintense on T2-weighted images; the remainder are isointense or hypointense. Most lesions are heterogeneous, demonstrating a combination of hyperintensity and hypointensity on T2-weighted images relative to hemorrhage and necrosis (Fig. 5a). One third of HAs have a peripheral rim corresponding to a fibrous capsule (81).

Dynamic Gd-enhanced MRI, whether performed with ECF agents or liver targeted agents, can demonstrate early arterial enhancement (although this usually is less marked than in cases of FNH) that becomes isointense or hypointense in the portal venous phase (Fig. 6a–d). In case of previous hemorrhage, the arterial enhancement can be inhomogeneous (Fig. 5b–e).

On delayed phase images after injection of Gd-BOPTA there is little evidence of uptake by HAs, which appear

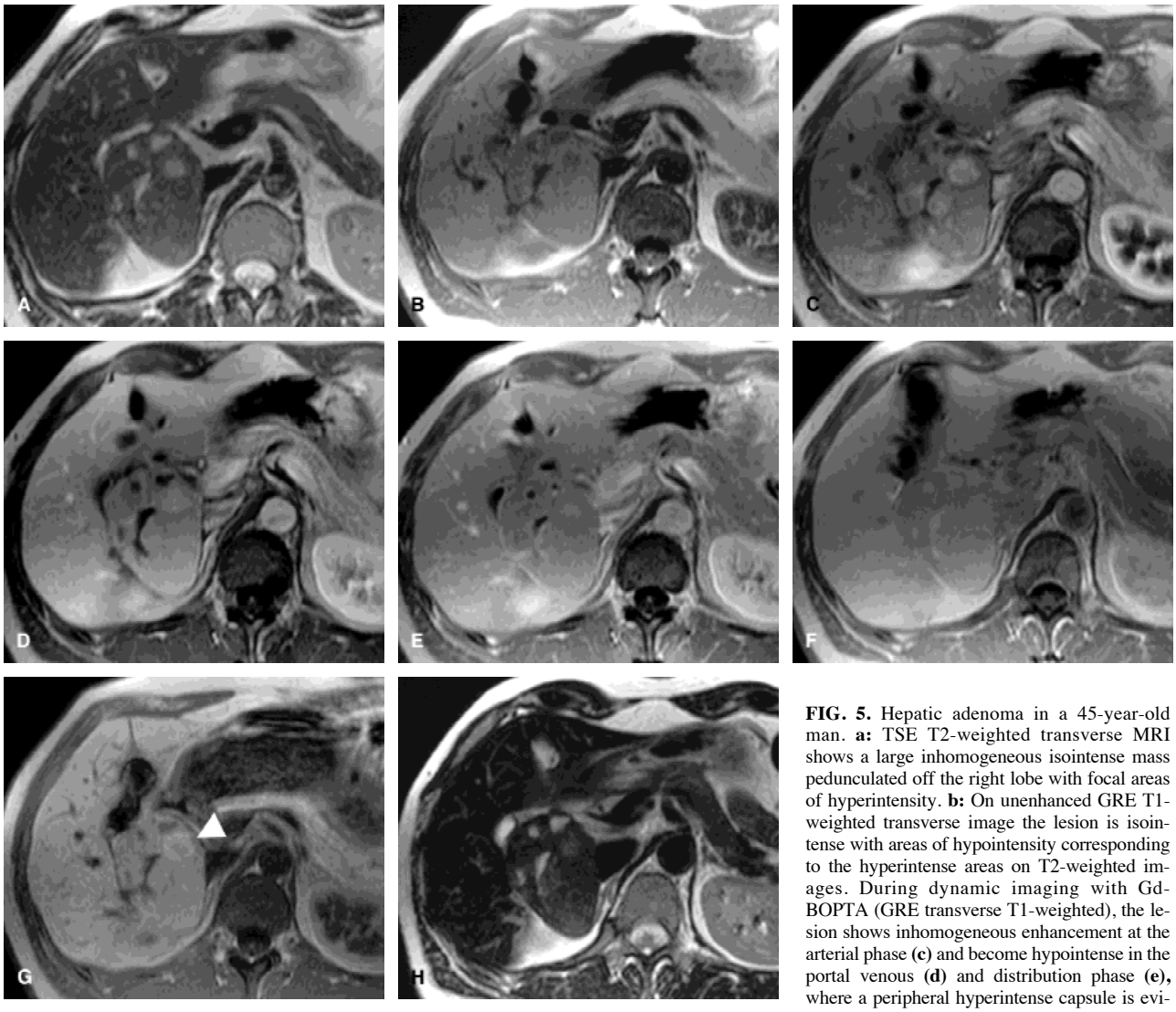


**FIG. 5.** Hepatic adenoma in a 45-year-old man. **a:** TSE T2-weighted transverse MRI shows a large inhomogeneous isointense mass pedunculated off the right lobe with focal areas of hyperintensity. **b:** On unenhanced GRE T1-weighted transverse image the lesion is isointense with areas of hypointensity corresponding to the hyperintense areas on T2-weighted images. During dynamic imaging with Gd-BOPTA (GRE transverse T1-weighted), the lesion shows inhomogeneous enhancement at the arterial phase **(c)** and become hypointense in the portal venous **(d)** and distribution phase **(e),** where a peripheral hyperintense capsule is evident. **f:** GRE transverse T1-weighted image at the hepatobiliary phase, 2 hours after Gd-BOPTA injection. The lesion appears slightly hypointense with areas of hyperintensity due to pooling of CM. **g:** GRE transverse T1-weighted 1 hour after Mn-DPDP injection. The lesion appears isointense with a spot of hyperintensity in one component of the lesion (arrowhead), corresponding to the hypervascular zone seen during the arterial phase (c). **h:** TSE T2-weighted transverse MRI 1 hour after injection of Endorem. Inhomogeneous signal drop of the lesion (compare with panel a) showing some areas of hyperintensity.

hypointense (Figs. 5f and 6e–f) (28). On the other hand, the hepatocellular-specific contrast agent Mn-DPDP is able to enter the abnormal hepatocytes, producing an isointense or hyperintense appearance on delayed phase images (Figs. 5g and 6g) (20).

HAs usually do not show uptake of SPIO particles, resulting in increased tumor-liver CNR on T2-weighted images (Fig. 6i). However, occasionally HAs have shown some degree of uptake (64), with a heterogeneous signal drop whose entity usually is lesser than in FNH (Fig. 5h). Uptake of SPIO in HA appears to be due to pooling of the contrast agent within the peliosis-like dilated vessels that characterize them (83). However, in several cases, no significant difference of signal loss was observed between FNH and HA (65).

In 1985 *liver adenomatosis* was described as a separate clinical entity, distinguished from isolated HA by the presence of multiple adenomas (arbitrarily, more than 10), lack of correlation with steroid medication, occurrence in both men and women, and abnormal increases in serum alkaline phosphatase and gamma-glutamyltransferase levels, in an otherwise normal liver and in patients without glycogen storage disease (84–87). Association with vascular anomalies have been described, such as portal ve-

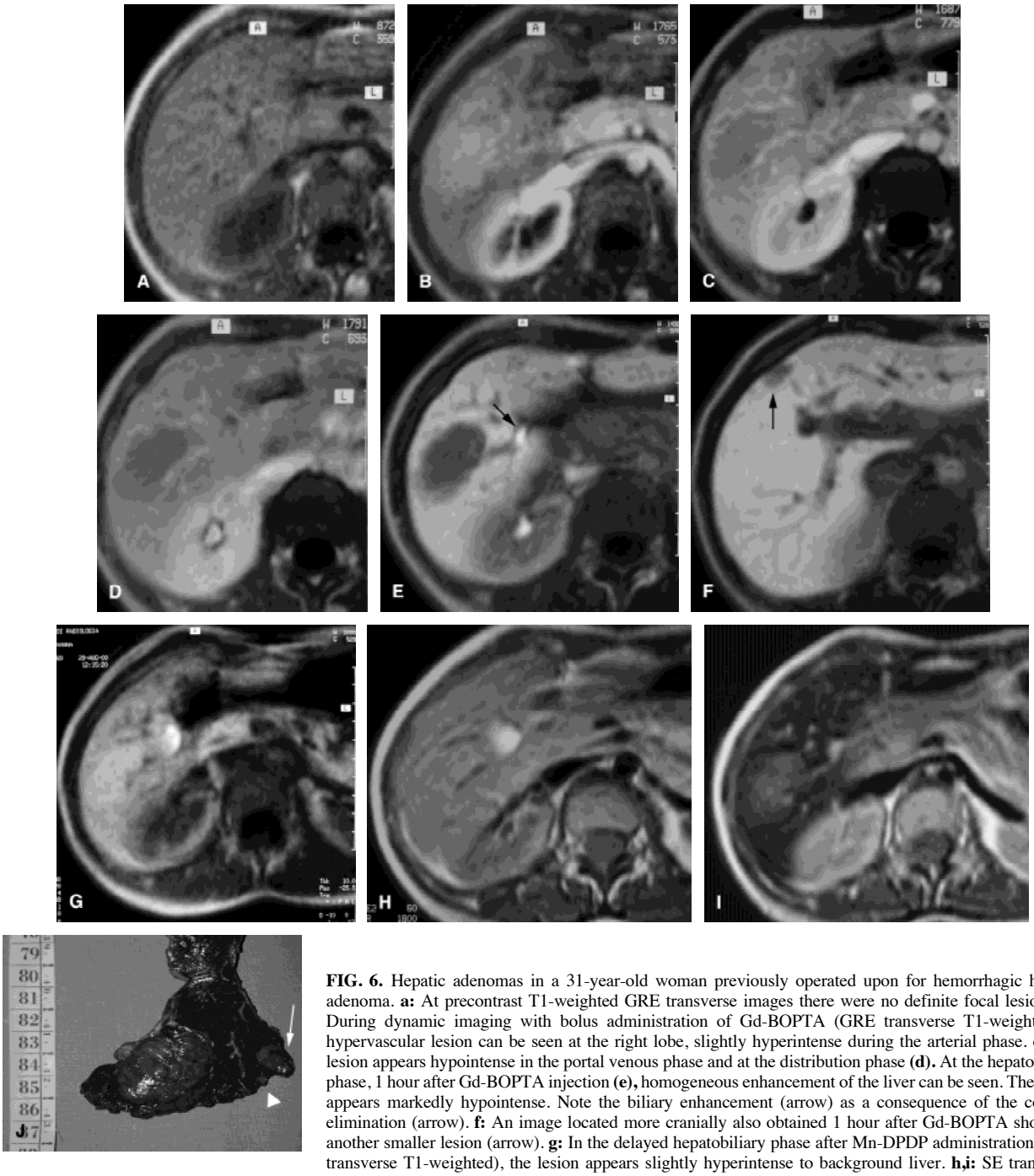

**FIG. 6.** Hepatic adenomas in a 31-year-old woman previously operated upon for hemorrhagic hepatic adenoma. **a:** At precontrast T1-weighted GRE transverse images there were no definite focal lesions. **b:** During dynamic imaging with bolus administration of Gd-BOPTA (GRE transverse T1-weighted), a hypervascular lesion can be seen at the right lobe, slightly hyperintense during the arterial phase. **c:** The lesion appears hypointense in the portal venous phase and at the distribution phase **(d).** At the hepatobiliary phase, 1 hour after Gd-BOPTA injection **(e),** homogeneous enhancement of the liver can be seen. The lesion appears markedly hypointense. Note the biliary enhancement (arrow) as a consequence of the contrast elimination (arrow). **f:** An image located more cranially also obtained 1 hour after Gd-BOPTA shows an another smaller lesion (arrow). **g:** In the delayed hepatobiliary phase after Mn-DPDP administration (GRE transverse T1-weighted), the lesion appears slightly hyperintense to background liver. **h,i:** SE transverse AU11 PD-weighted image before (h) and 1 hour after (i) the administration of Endorem. **h:** No lesion can be seen. **i:** Homogeneous signal drop is observed throughout the liver. The lesion shows a lack of SPIO uptake; thus, it appears hyperintense to the surrounding liver parenchyma. **j:** Surgical specimen. The large lesion and the small lesion (arrow) seen on MRI can be appreciated. Another smaller lesion can be seen at pathology (arrowhead).

nous thrombosis, congenital absence of the portal vein, and portosystemic venous shunt (88).

Histologically, the lesions consist of sheets of hepatocytes with foamy cytoplasm and uniform round nuclei. Portal tracts and bile ducts are absent, but Kupffer cells and fatty components can be present in some of the nodules. Many of the nodules show evidence of subacute or chronic hemorrhage. According to Chiche et al. (89), two different forms of liver adenomatosis can be distinguished: massive and multifocal. Of these two types, the

former has an increased risk of malignant degeneration and hemorrhage. The natural history and pathogenesis of liver adenomatosis are unclear. Because of the chance of malignant degeneration and hemorrhage, resection of adenomas is warranted in many cases, even if some smaller adenomas remain in place (84,85). Orthotopic liver transplantation may be reserved for patients who have progressive signs or symptoms after partial resection or in those in whom HCC is suspected (88).

MRI shows variable lesion heterogeneity and signal intensity. In general the images appear similar to hepatic adenomas as previously described. On T2-weighted images, most of the adenomas are heterogeneously moderately hyperintense or homogeneously isointense (Fig. 7a). Noncomplicated lesions are generally isointense to the liver parenchyma on T1-weighted images (Fig. 7b). Intratumoral fat is heterogeneously hyperintense on T1-weighted images, whereas intratumoral hemorrhage, when present, appears heterogeneously hyperintense on T1-weighted and T2-weighted images. In opposed-phase chemical shift imaging, lesions show signal dropout, which is indicative of lipid content.

On Gd-enhanced MRI most adenomas are hyperintense on arterial and early portal venous phase images, whereas on late portal venous phase images and equilibrium phase images most appear isointense or homogeneously hypointense (Fig. 7c–e). On delayed phase images after injection of Gd-BOPTA most lesions appear hypointense, indicating a lack of uptake by the lesions (Fig. 7f). On the other hand, Mn-DPDP is able to enter the abnormal hepatocytes, resulting in a hyperintense appearance on delayed phase images (Fig. 7g). After intravenous administration

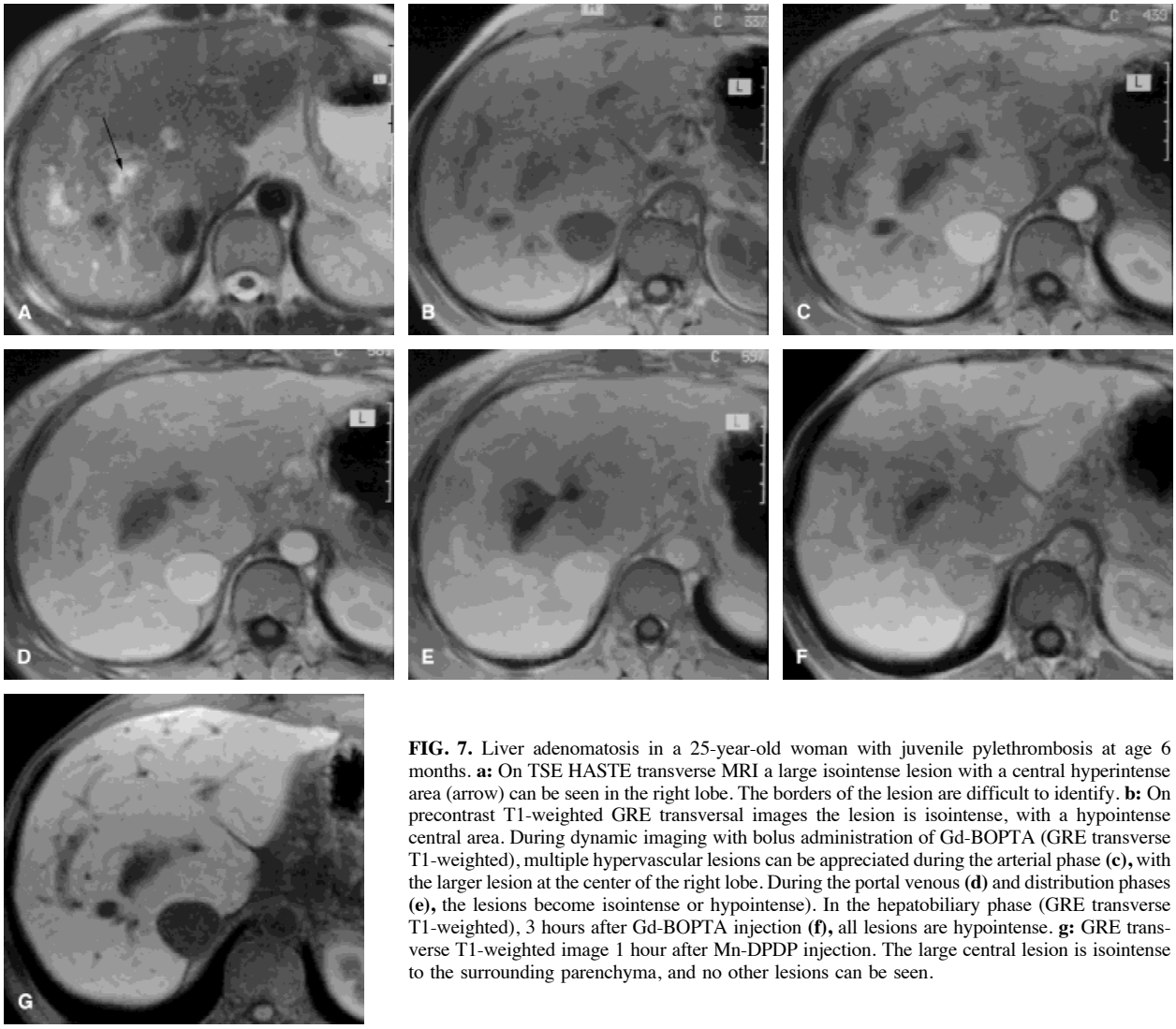


**FIG. 7.** Liver adenomatosis in a 25-year-old woman with juvenile pylethrombosis at age 6 months. **a:** On TSE HASTE transverse MRI a large isointense lesion with a central hyperintense area (arrow) can be seen in the right lobe. The borders of the lesion are difficult to identify. **b:** On precontrast T1-weighted GRE transversal images the lesion is isointense, with a hypointense central area. During dynamic imaging with bolus administration of Gd-BOPTA (GRE transverse T1-weighted), multiple hypervascular lesions can be appreciated during the arterial phase **(c),** with the larger lesion at the center of the right lobe. During the portal venous **(d)** and distribution phases **(e),** the lesions become isointense or hypointense). In the hepatobiliary phase (GRE transverse T1-weighted), 3 hours after Gd-BOPTA injection **(f),** all lesions are hypointense. **g:** GRE transverse T1-weighted image 1 hour after Mn-DPDP injection. The large central lesion is isointense to the surrounding parenchyma, and no other lesions can be seen.

of ferumoxides particles, adenomas show variable uptake of the contrast material, with lesion conspicuity decreasing at intermediate-weighted and T2-weighted imaging.

**Malignant focal liver lesions: Hepatocyte origin**

*HCC* is the most frequent primary tumor of the liver (80%–90%) and represents more than 5% of all cancers, with an incidence of more than 500,000 new cases per year throughout the world (90). Its incidence in developing countries is two to three times higher than in developed countries, although its incidence is rising in western countries and in Japan (91). The most significant risk factor, regardless of etiology, is the presence of liver cirrhosis (92), particularly when secondary to viral infection and high alcohol intake. Other risk factors include hemochromatosis and primary biliary cirrhosis (90).

HCC is the endpoint of a serial transformation beginning from a dysplastic nodule. HCC can develop from a dysplastic nodule in as few as 4 months (93–95). According to the terminology of an international working party in 1994, there are three steps in the development of HCC: regenerative nodule, dysplastic nodule (low grade; high grade; with focus of HCC), and small HCC (less than 2 cm) (96).

Regenerative nodules are benign lesions with exclusive portal venous blood supply and represent a nonspecific response to a variety of insults to the liver. Low-grade dysplastic nodules show slight cytologic atypia, mainly large cell changes, whereas high-grade dysplastic nodules are premalignant lesions that can demonstrate enhancement during the arterial phase on MRI and CT. These lesions can be diagnosed incorrectly as HCC when arterial phase enhancement is seen, although this is a rare circumstance for dysplastic nodules (97,98).

Considered premalignant lesions, dysplastic nodules pose a higher risk for development of HCC in patients with than those without dysplastic nodules. In about one third of high-grade dysplastic nodules small foci of carcinomas can be found; thus these nodules are termed "dysplastic nodules with focus of HCC."

Dysplastic nodules have been described as demonstrating hyperintensity on T1-weighted images and hypointensity on T2-weighted images (99,100). Although arterial phase enhancement as a criterion for dysplastic nodule can increase the sensitivity for characterization, this is at the expense of decreased specificity because of the overlap with the much more commonly seen arterial phase enhancement in HCC (97). When HCC elements are found in a lesion smaller than 2 cm, they are called "small HCC." These lesions demonstrate arterial phase enhancement more frequently than dysplastic nodules on all imaging modalities.

The macroscopic appearance of HCC has been classified as expanding, spreading, and multifocal. According to Edmondson and Steiner (101), HCCs can be classified from grades I to IV based on histologic differentiation. A frequent observation, particularly in small HCC, is fatty degeneration.

The formation of a pseudocapsule around the lesion (constructed usually from connective fibrous tissue) and of a septum within the tumor is frequently observed with the development of HCC. This may derive from an interaction between tumor and host liver and may interfere with the growth and invasion of the HCC (102).

Kupffer cells are present in HCCs. Although there are no statistically significant differences in the numbers of Kupffer cells between small well-differentiated HCCs and noncancerous tissues, the numbers tend to decrease in cancerous tissues compared with noncancerous tissues as tumor size increases and histologic grade decreases (103).

Many factors affect the visualization of primary focal hepatic lesions during unenhanced and/or contrast-enhanced MRI of the liver, e.g., the dimensions, composition and degree of vascularization of the lesion, the functionality of the normal hepatic parenchyma, and the residual hepatic functionality of the neoplastic cells themselves. Unfortunately such factors tend to vary from patient to patient, often making the behavior of a given HCC lesion difficult to predict. Previous studies aimed at correlating the appearance of HCC on MRI with the pathologic characteristics of the lesion reflect the difficulty in drawing firm conclusions on the behavior of such lesions (99,104–107).

HCCs are mildly to moderately hyperintense at turbo T2-weighted and/or STIR imaging (Figs. 8a and 9a). On F8 T1-weighted images increased signal intensity (Fig. 9b) F9 correlates with a more well-differentiated histologic grade than does isointensity or hypointensity (97,108). Hyperintensity on T1-weighted images is related to several factors, such as fatty metamorphosis, glycogen, clear cells, and copper (109).

Dynamic T1-weighted imaging during the arterial phase is of utmost importance for the detection of small HCCs, because they may be occult at other pulse sequences and on portal venous and equilibrium phase images (97). Typically HCCs demonstrate arterial enhancement at dynamic imaging (Figs. 8 and 9).

Yamashita et al. (106) demonstrated a correlation between tumor grade and peak contrast enhancement on dynamic Gd-DTPA–enhanced gradient-echo FLASH images with a lower peak enhancement for smaller and well-differentiated lesions. They also reported a statistical correlation between peak contrast enhancement of the lesion and an increased dilation of sinusoid-like spaces in

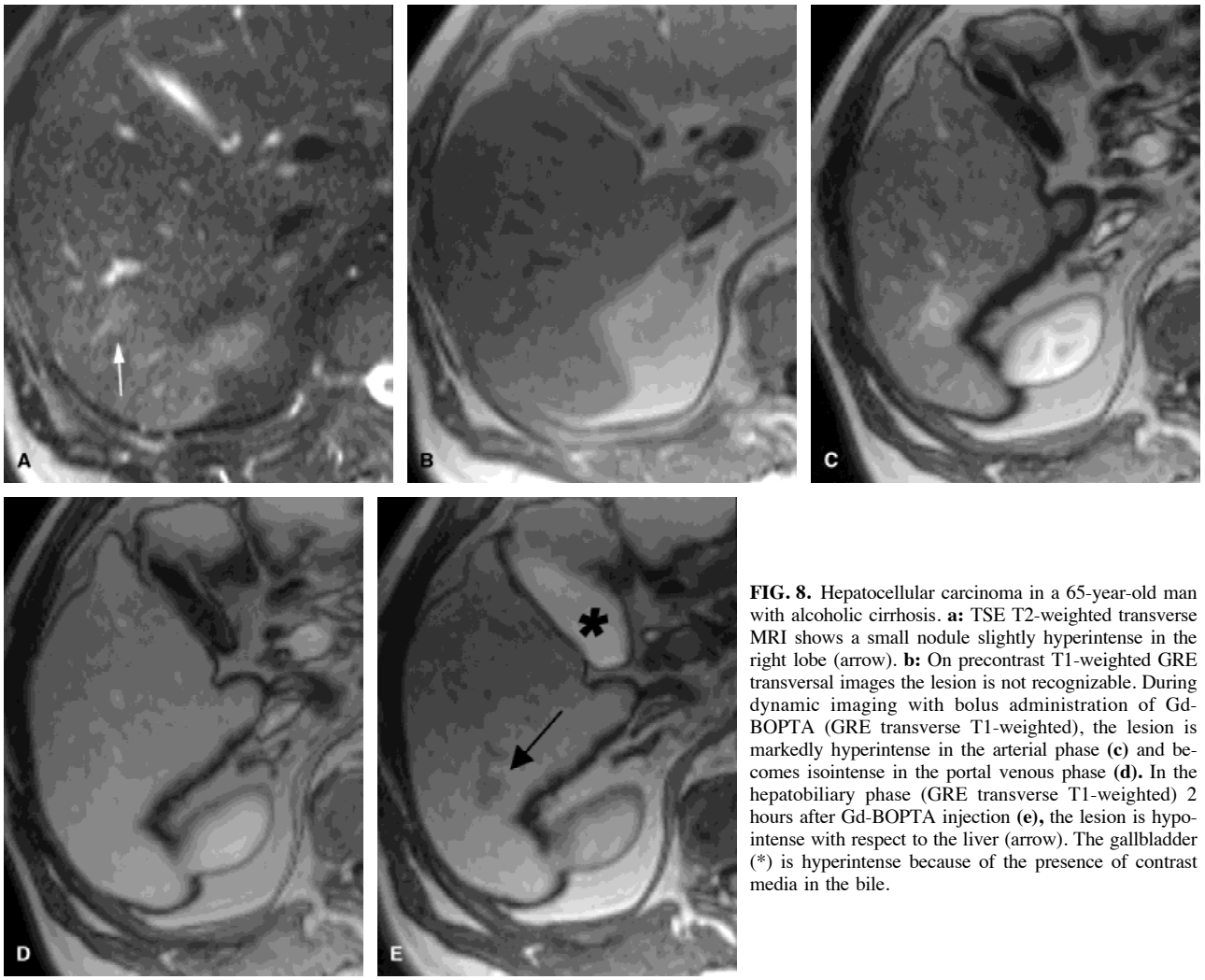


**FIG. 8.** Hepatocellular carcinoma in a 65-year-old man with alcoholic cirrhosis. **a:** TSE T2-weighted transverse MRI shows a small nodule slightly hyperintense in the right lobe (arrow). **b:** On precontrast T1-weighted GRE transversal images the lesion is not recognizable. During dynamic imaging with bolus administration of Gd-BOPTA (GRE transverse T1-weighted), the lesion is markedly hyperintense in the arterial phase **(c)** and becomes isointense in the portal venous phase **(d).** In the hepatobiliary phase (GRE transverse T1-weighted) 2 hours after Gd-BOPTA injection **(e),** the lesion is hypointense with respect to the liver (arrow). The gallbladder (*) is hyperintense because of the presence of contrast media in the bile.

moderately/poorly differentiated HCC as opposed to well-differentiated HCC. This suggests a higher accumulation of contrast agent in the sinusoid-like spaces of moderately/poorly differentiated HCCs compared with well-differentiated HCCs in the arterial phase of contrast enhancement. However, these findings should be interpreted with caution because controversies regarding the optimal timing to capture the arterial phase exist (110–112) and may influence attempts to reproduce the results.

The pseudocapsule of HCC appears hypointense on unenhanced T1-weighted and T2-weighted spin-echo and gradient-echo MRI sequences. On contrast-enhanced MRI the enhancement is more evident on arterial phase images but may persist into the equilibrium phase (Fig. 9e) (113).

Lesion enhancement is observed after injection of paramagnetic contrast agents with liver-specific properties. In an anecdotal case of high-grade dysplastic nodule examined with Gd-BOPTA, the lesion was hyperintense to the surrounding liver parenchyma at the hepatobiliary phase (Fig. 10). F10

Dynamic imaging of HCC with Gd-BOPTA is similar to that observed with conventional vascular-interstitial CM (Figs. 8 and 9). Delayed phase imaging (about 1 hour after injection) reveals a number of different enhancement patterns, with isointense, hypointense, and hyperintense patterns possible (Figs. 8e, 9f, and 11e). F11

In a previous study we revealed a tendency for moderately differentiated lesions to enhance to a greater extent on delayed images compared with both well-differentiated lesions and poorly differentiated lesions, although statistical significance was not demonstrated for any of these differences (114). In a retrospective analysis of 94 HCCs with Gd-BOPTA, 89.4% were hypointense in the delayed phase, whereas only 3.2% and 7.4% were hyperintense and isointense, respectively (115). Manfredi et al. (27) demonstrated that well-differentiated and moderately dif-

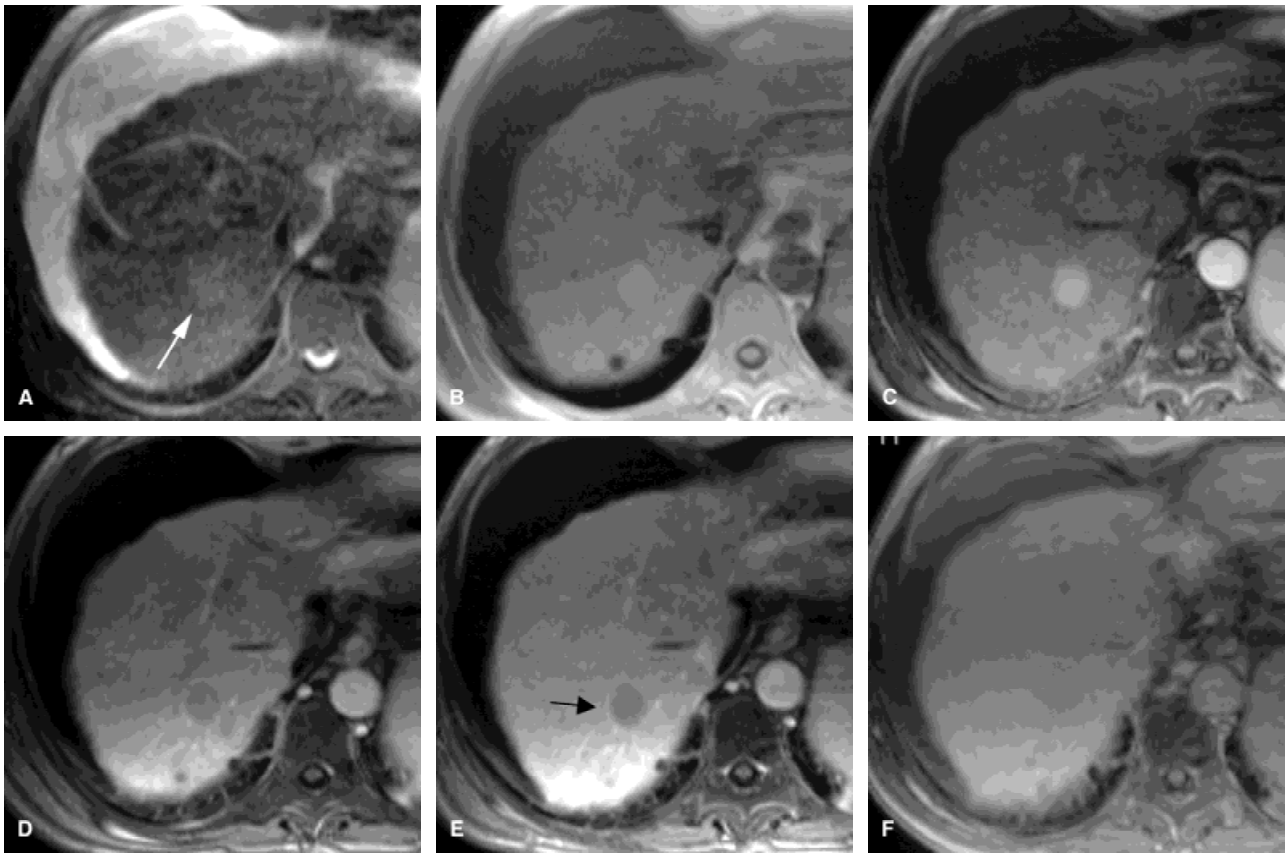


**FIG. 9.** Hepatocellular carcinoma in a 53-year-old man with alcoholic cirrhosis. **a:** TSE T2-weighted transverse MRI shows a small nodule slightly hyperintense in the right lobe (arrow). **b:** On precontrast T1-weighted GRE transversal images the lesion is hyperintense. During dynamic imaging with bolus administration of Gd-BOPTA (GRE transverse T1-weighted), the lesion is hyperintense in the arterial phase **(c)** to become hypointense in the portal venous **(d)** and distribution phase **(e).** In this phase a peripheral capsule is well evident (arrow). **f:** In the hepatobiliary phase (GRE transverse T1-weighted) 2 hours after Gd-BOPTA injection the lesion is isointense.

ferentiated HCC show superior signal enhancement ratios than poorly differentiated HCC on images acquired on a 0.5-T machine at 60 to 120 minutes after Gd-BOPTA administration. This finding reflects the retention of sufficient hepatocytic activity by these lesions to take up Gd-BOPTA. A significant correlation was observed between the presence of intralesional bile and the degree of enhancement of the lesions after Gd-BOPTA administration (114).

With the hepatobiliary agent Mn-DPDP, all hepatocellular tumors demonstrate enhancement, with HCCs frequently showing inhomogeneous enhancement (Fig. 12) (19). Well-differentiated HCC enhance to a greater extent than poorly differentiated HCC (17). A rim-like enhancement on Mn-DPDP–enhanced MRI can be seen in HCC, whose underlying mechanism has been attributed to several causes. Peritumoral malignant infiltration into neighboring normal liver parenchyma can result in intermingling of nonhepatocellular malignant cells with normal functioning hepatocytes in the peripheral region of liver metastasis.

However, such a finding also has been in cholangiocarcinoma (116) and metastases (18), resulting from compression of surrounding normal liver tissue by a metastatic tumor mass. This compression may have led to impaired Mn-DPDP excretion or persistent Mn-DPDP retention because of compressed bile canaliculi in these areas (117). This finding leads to difficulties in differentiating metastases from poorly differentiated HCC.

MRI after Mn-DPDP administration has been shown to result in more accurate differentiation between benign (FNH) and malignant (HCC) hepatocellular tumors than unenhanced MRI, although absolute values for sensitivity, specificity, and accuracy were not particularly satisfactory (64.5%, 66.7%, and 65.1%, respectively) (118). A study aimed at determining the efficacy of Mn-DPDP for the evaluation of HCC revealed low overall efficacy for Mn-DPDP–enhanced MRI compared with unenhanced MRI

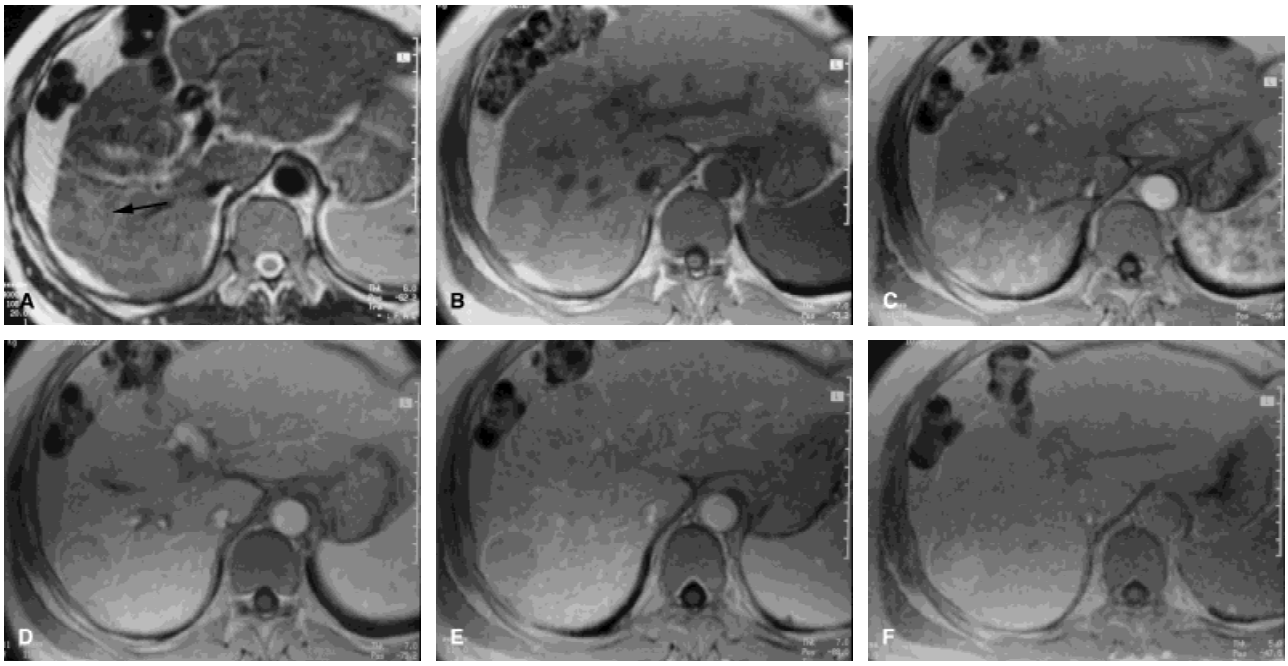


**FIG. 10.** High-grade dysplastic nodule in a 56-year-old man with cirrhosis. **a:** TSE T2-weighted transverse MRI shows a round isointense nodule with some slightly hyperintense areas in the right lobe (arrow). **b:** On precontrast T1-weighted GRE transverse images the lesion is hyperintense. During dynamic imaging with bolus administration of Gd-BOPTA (GRE transverse T1-weighted), the lesion shows inhomogeneous enhancement in the arterial phase **(c)** to become hypointense in the portal venous **(d)** and distribution phase **(e),** with a peripheral capsule. **f:** In the hepatobiliary phase (GRE transverse T1-weighted) 2 hours after Gd-BOPTA injection the lesion is hyperintense.

for the identification of lesions (49 lesions in 20 patients for Mn-DPDP–enhanced MRI compared with 50 lesions in 17 patients for unenhanced MRI) (17).

With SPIO particles, HCCs generally do not show a significant decrease in signal intensity, although signal intensity loss was seen in some individual HCCs (64). The signal intensity of the normal liver does decrease, however, thereby improving the CNR of malignant focal liver lesions (Fig. 13).

According to Lim et al. (119), HCC conspicuity after SPIO depends on differences in the number of Kupffer cells between the lesion and the surrounding cirrhotic liver. Moderately or poorly differentiated HCCs show large differences in the number of Kupffer cells compared with the surrounding cirrhotic liver and thus demonstrate a high CNR at SPIO-enhanced MRI. Dysplastic nodules and most well-differentiated HCCs, on the other hand, contain nearly the same number of Kupffer cells as the surrounding cirrhotic hepatic parenchyma and therefore are not well depicted on T2-weighted MR images (119). Tang et al. (120) found significantly more lesions on Gd-enhanced MRI compared with ferumoxides-enhanced MRI in 53 patients (97/103 versus 80/103, $p < 0.01$) On the other hand, Vogl et al. (121) detected more HCCs with ferumoxides-enhanced MRI than with dynamic Gd-enhanced MRI. As with Mn-DPDP, the lack of a dynamic imaging capability limits the possibilities for lesion characterization with SPIO-enhanced MRI. This problem can be overcome with the new SPIO agent SHU 555 A (Fig. 13) or, when available, USPIO.

Some authors have proposed the possibility of a single-visit sequential SPIO-Gd protocol to obtain better diagnostic confidence (122). Ward et al. (123) found that the combination of Gd and ferumoxides in double-contrast MRI, compared with ferumoxides-enhanced imaging alone, led to an improvement in the diagnosis of HCC, especially for small lesions (less than 1 cm), for which the sensitivity for detection increased from 14% to 46%, compared with larger lesions (1 cm or larger), for which the sensitivity increased from 81% to 91% with the addition of Gd-enhanced imaging. Post–Gd-enhanced images obtained during the arterial and portal phases of enhancement were essential for differentiating HCC from adjacent fibrosis, which is the most frequent cause of false-positive findings of SPIO-enhanced and SPIO-unenhanced images.

Pauleit et al. (124) found that for detection of small HCCs, the sensitivity and accuracy with unenhanced and Gd-enhanced imaging were significantly ($p = 0.017$) superior to those with unenhanced and ferumoxides-enhanced imaging, whereas for large HCCs the ferumoxides set was superior to the Gd set, although this difference was not statistically significant. Analysis of all HCCs re-

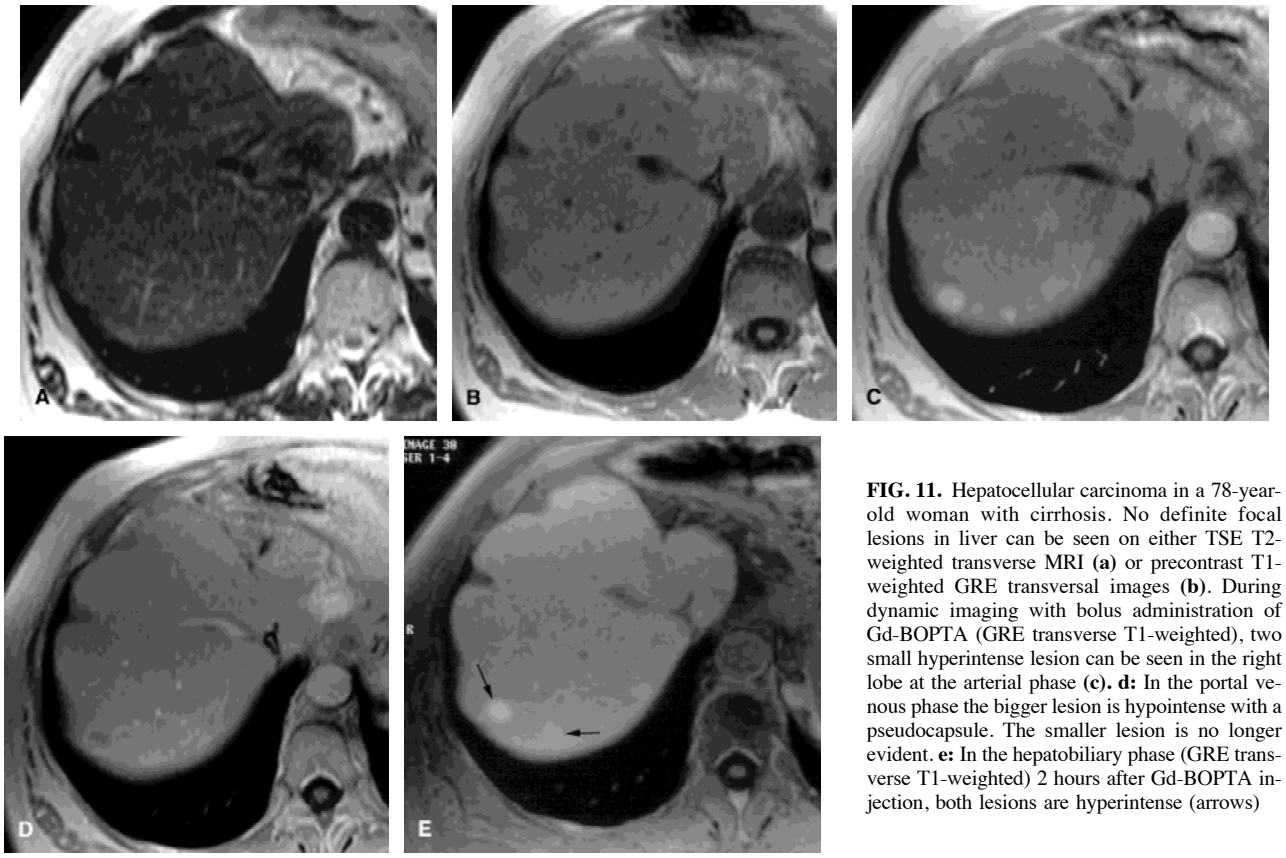


**FIG. 11.** Hepatocellular carcinoma in a 78-year-old woman with cirrhosis. No definite focal lesions in liver can be seen on either TSE T2-weighted transverse MRI **(a)** or precontrast T1-weighted GRE transversal images **(b)**. During dynamic imaging with bolus administration of Gd-BOPTA (GRE transverse T1-weighted), two small hyperintense lesion can be seen in the right lobe at the arterial phase **(c). d:** In the portal venous phase the bigger lesion is hypointense with a pseudocapsule. The smaller lesion is no longer evident. **e:** In the hepatobiliary phase (GRE transverse T1-weighted) 2 hours after Gd-BOPTA injection, both lesions are hyperintense (arrows)

vealed no significant differences for Gd-enhanced and ferumoxides-enhanced imaging (124).

*Fibrolamellar HCC* was first described by Edmonson and Steiner (101). Fibrolamellar HCC is a sharply defined, lobulated, nonencapsulated tumor, whose characteristic microscopic features include fibrolamellar bands of collagen and fibrocytes arranged in a lamellar pattern and in delicate bands between nests of tumor cells, which often coalesce to form a central scar (125). Typically, fibrolamellar HCCs occurs in a noncirrhotic liver, primarily in young adults with no clear gender predominance (126).

On CT and MRI the majority of tumors demonstrate hypervascularity with an inhomogeneous pattern. A central scar is seen in about 71% of the cases with absent or

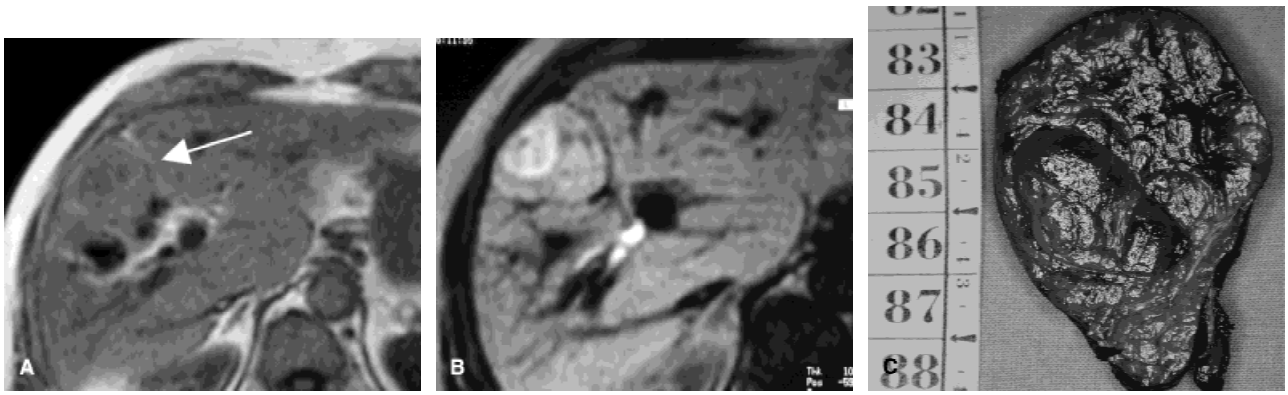


**FIG. 12.** Well-differentiated hepatocellular carcinoma in a patient with chronic hepatitis evaluated with Mn-DPDP. **a:** On precontrast T1-weighted GRE image a isointense nodule can be seen in the right lobe (arrow). **b:** After Mn-DPDP administration the lesion becomes inhomogeneously hyperintense, with a marked hyperintense eccentric focus. c: Pathologic specimen from which the histologic diagnosis was made.

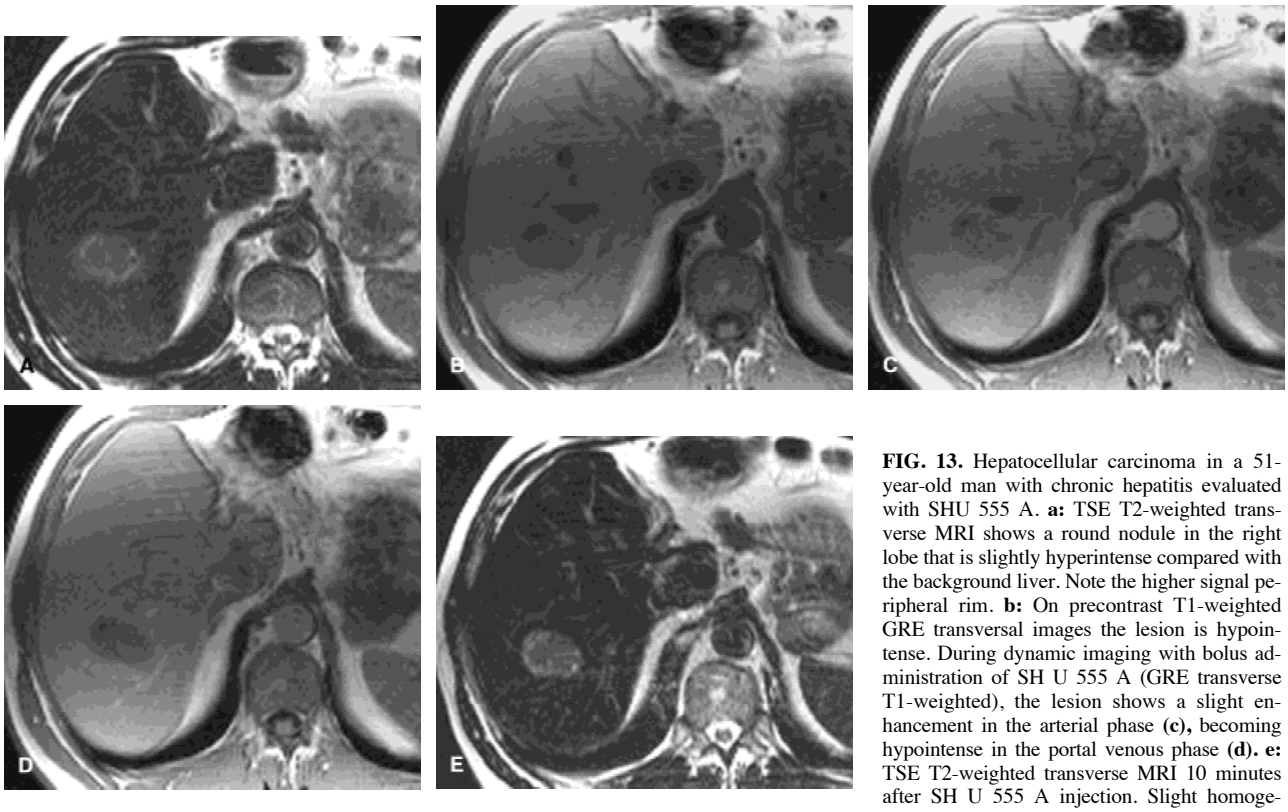


**FIG. 13.** Hepatocellular carcinoma in a 51-year-old man with chronic hepatitis evaluated with SHU 555 A. **a:** TSE T2-weighted transverse MRI shows a round nodule in the right lobe that is slightly hyperintense compared with the background liver. Note the higher signal peripheral rim. **b:** On precontrast T1-weighted GRE transversal images the lesion is hypointense. During dynamic imaging with bolus administration of SH U 555 A (GRE transverse T1-weighted), the lesion shows a slight enhancement in the arterial phase **(c),** becoming hypointense in the portal venous phase **(d). e:** TSE T2-weighted transverse MRI 10 minutes after SH U 555 A injection. Slight homogeneous signal drop is observed throughout the liver parenchyma. The lesion shows a lack of contrast media uptake; thus, it appears more hyperintense compared with the surrounding liver parenchyma.

minimal contrast enhancement. Calcifications are found in 68% of lesions with CT, almost always within the central scar, whereas hemorrhage and necrosis are rarely found. The fibrous tissue within the scar and radial septa demonstrate persistent enhancement on contrast-enhanced CT and MRI obtained 10 to 20 minutes after contrast material administration (125). In our experience of three cases of fibrolamellar HCC imaged with Gd-BOPTA–enhanced MRI, none of the tumors showed delayed enhancement 1 to 3 hours after contrast administration.

With Mn-DPDP, tumor enhancement was seen in one of three fibrolamellar HCC cases, giving an overall isointense appearance, but enhancement was not in the remaining two cases (125). Lymph node enhancement in metastatic fibrolamellar carcinoma after administration of Mn-DPDP has been reported (127). To our knowledge, there are no reports of Fl-HCC enhancement patterns after SPIO. Such lesions would not be expected to enhance significantly.

**Benign nonhepatocytic focal lesions**

*Capillary hemangiomas* are rapidly filling hemangiomas that occur significantly more often in small hemangiomas (42% of hemangiomas less than 1 cm in diameter) (128). On CT and MRI, capillary hemangiomas show immediate homogeneous enhancement in the arterial phase; thus, differentiation from other hypervascular tumors is difficult. According to various authors, up to 83% of the smaller hemangiomas (less than 3 cm) showed isoattenuation compared with the arterial system in all three phases of enhanced scanning (Fig. 14) (129,130). F14

Hyperintensity on T2-weighted images has been relied upon by some to establish the diagnosis of hemangioma, although it must be remembered that on heavily T2-weighted sequences with long echo delay times, high signal intensity lesions may be produced by some hypervascular metastases, such as sarcoma, islet cell tumor, pheochromocytoma, carcinoid (Fig. 15a), and renal cell F15 carcinoma (Fig. 16a). F16

During the portal venous phase of contrast enhancement, capillary hemangiomas shows an attenuation equivalent to that of the aorta. In the distribution phase, CT or MRI hemangiomas remain hyperattenuating or hyperintense, whereas hypervascular metastases do not (131). The MR findings with liver-specific contrast agents are discussed in the section of cavernous hemangioma, which is found in the section of focal liver lesions with delayed persistent enhancement.

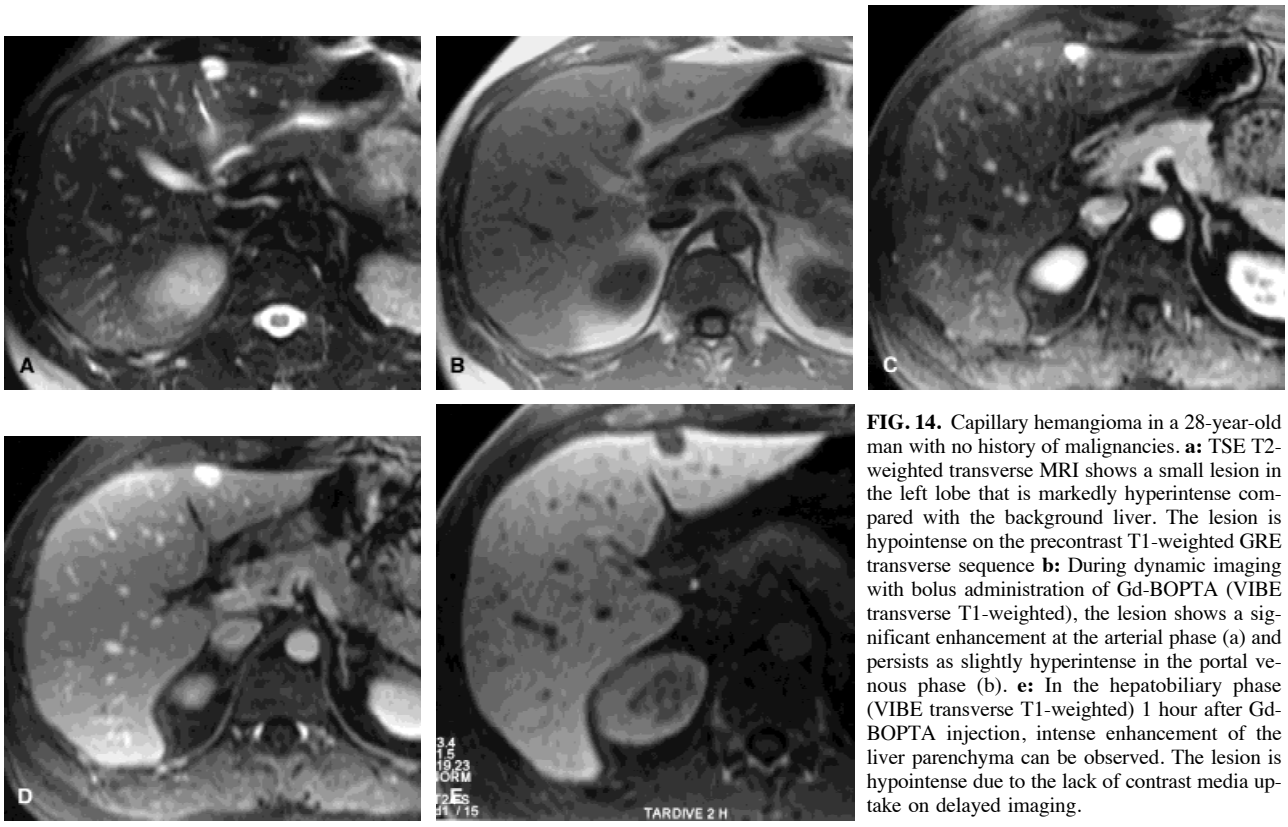


**FIG. 14.** Capillary hemangioma in a 28-year-old man with no history of malignancies. **a:** TSE T2-weighted transverse MRI shows a small lesion in the left lobe that is markedly hyperintense compared with the background liver. The lesion is hypointense on the precontrast T1-weighted GRE transverse sequence **b:** During dynamic imaging with bolus administration of Gd-BOPTA (VIBE transverse T1-weighted), the lesion shows a significant enhancement at the arterial phase (a) and persists as slightly hyperintense in the portal venous phase (b). **e:** In the hepatobiliary phase (VIBE transverse T1-weighted) 1 hour after Gd-BOPTA injection, intense enhancement of the liver parenchyma can be observed. The lesion is hypointense due to the lack of contrast media uptake on delayed imaging.

AU12

**Malignant nonhepatocytic focal lesions**

*Hypervascular metastases* derive from highly vascular tumors, such as carcinoid, islet cell tumor, renal carcinoma, thyroid carcinoma, pheochromocytoma, melanoma, and breast carcinoma. On unenhanced images, when compared with background liver tissue these lesions usually are hypointense on T1-weighted images and slightly hyperintense and/or heterogeneous in SI on T2-weighted images. As mentioned previously, some hypervascular metastases tend to have higher SI on T2-weighted images and may mimic hemangiomas (Figs. 15a and 16a) (132,133).

These lesions show significant enhancement during the arterial phase of ECF agent contrast enhancement, which is the most important phase for lesion detection (Fig. 15c), whereas hypovascular lesions are best imaged during the portal phase. The equilibrium phase is best used for lesion characterisation rather than detection, by analyzing the pattern of enhancement and degree of contrast wash-out. In the portovenous phase these lesions may become isointense with the normal liver parenchyma. Larger hypervascular metastases receive arterial blood mainly in the periphery of the lesion than in the less perfused center and thus shows a peripheral rim of enhancement (Fig. 16c) (132,133).

In the portovenous phase these lesions usually show some rapid washout, which renders them slightly lower in density than the surrounding normal liver parenchyma. On delayed phase the CM accumulates in the center of the lesion because of its pooling in the extracellular fibrotic component of the lesion, thus becoming progressively hyperintense to the surrounding liver parenchyma (delayed central pooling). At the periphery of the lesion the clearance of CM is faster than the normal surrounding liver parenchyma (peripheral washout), thus giving an hypointense halo because the enhancement prevails within the central zone of the metastasis and within the perilesional hepatic tissue (134). The latter finding of peripheral washout is specific for metastases but is a relatively uncommon finding, as discussed later. When T2 signal intensity is high, mimicking hemangioma, inhomogeneous signal intensity on unenhanced images, early washout, delayed central pooling, and multiple lesions are suggestive for the metastatic nature of the lesion.

The dynamic enhancement with Gd-BOPTA–enhanced dynamic MRI is superimposable with the patterns seen with ECF Gd-based contrast agents. However in the late hepatobiliary phase (about 1 hour after Gd-BOPTA injection), all metastases appear hypointense to the surrounding hyperintense background liver parenchyma (Figs. 15e and 16e). It should be stressed that 1 hour after the injection of

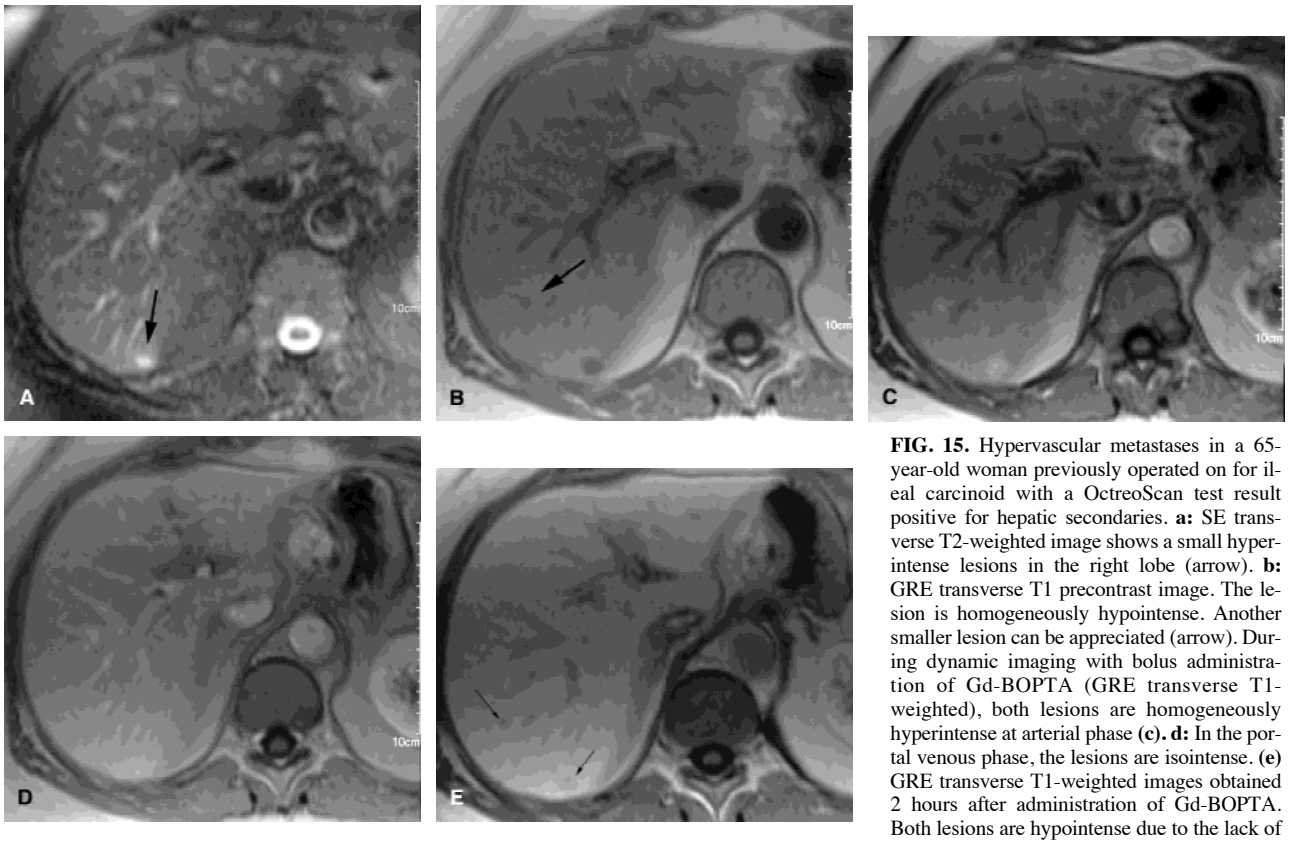


**FIG. 15.** Hypervascular metastases in a 65-year-old woman previously operated on for ileal carcinoid with a OctreoScan test result positive for hepatic secondaries. **a:** SE transverse T2-weighted image shows a small hyperintense lesions in the right lobe (arrow). **b:** GRE transverse T1 precontrast image. The lesion is homogeneously hypointense. Another smaller lesion can be appreciated (arrow). During dynamic imaging with bolus administration of Gd-BOPTA (GRE transverse T1-weighted), both lesions are homogeneously hyperintense at arterial phase **(c). d:** In the portal venous phase, the lesions are isointense. **(e)** GRE transverse T1-weighted images obtained 2 hours after administration of Gd-BOPTA. Both lesions are hypointense due to the lack of contrast media uptake.

Gd-BOPTA, some pooling of CM can be observed in the center of the lesion, secondary to its accumulation in the extracellular space of the lesion, thus mimicking hepatocytic accumulation. In such cases, it can be useful to repeat the sequence 2 to 3 hours. after the injection, when a complete washout of the CM from the interstitial space has been obtained.

After Mn-DPDP infusion, hypervascular metastatic lesions typically appear hypointense to the surrounding liver parenchyma, the latter higher in signal. However, uptake of $Mn^{2+}$ after Mn-DPDP infusion also has been observed in hepatic metastases from nonfunctioning endocrine tumors of the pancreas (16).

After SPIO, there is no significant uptake of CM; thus, the lesion appears hyperintense to the low signal intensity of the surrounding normal liver parenchyma on T2-weighted or T2*-weighted images. The rapid injection AU4 possible with SHU 555 allows one to observe both dynamic and RES phases, thus facilitating lesion character- F17 ization (Fig. 17).

Among solid *hypovascular liver lesions,* metastases are the main group. *Hepatic metastases* are the most frequent malignancies in the liver. The incidence of hepatic metastases is approximately 40% in patients with colorectal cancer (135). In the United States, approximately 50,000 cases of hepatic colorectal metastases are seen annually (136). Lesion detection is size related. An accepted lower threshold for detection is about 1 cm (137). Unfortunately, postmortem assessment of the size of liver metastases has shown that the ratio between metastases larger than 1 cm and those smaller than 1 cm is approximately 1:1.6 for metastases of colorectal adenocarcinoma and 1:4 for other liver metastases (138). This clearly indicates that a capacity to accurately detect and characterize metastases smaller than 1 cm is necessary.

The gross morphology of liver metastases, their localization, and their number show a wide range of variability (139,140). Metastatic lesions tend to be round, but metastases from colorectal adenocarcinoma larger than 3 cm commonly have a cauliflower aspect (Figs. 18 and 19) F18,F19 (141). The signal intensity of the metastases is lower than surrounding hepatic tissue on T1-weighted images but is higher on T2-weighted images.

Liquefactive necrosis within the metastasis increases signal intensity on T2-weighted images, whereas coagulative necrosis (142), desmoplastic reaction, or calcifica-

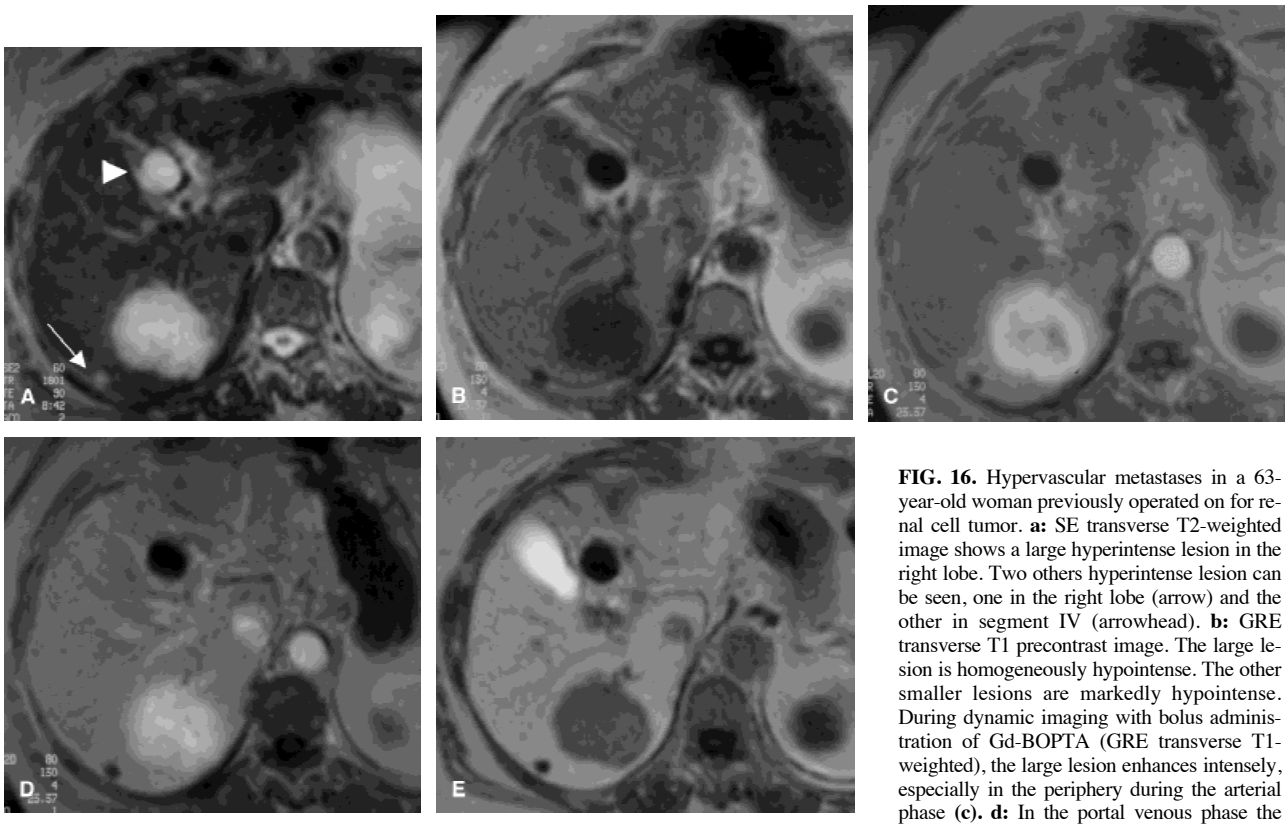


**FIG. 16.** Hypervascular metastases in a 63-year-old woman previously operated on for renal cell tumor. **a:** SE transverse T2-weighted image shows a large hyperintense lesion in the right lobe. Two others hyperintense lesion can be seen, one in the right lobe (arrow) and the other in segment IV (arrowhead). **b:** GRE transverse T1 precontrast image. The large lesion is homogeneously hypointense. The other smaller lesions are markedly hypointense. During dynamic imaging with bolus administration of Gd-BOPTA (GRE transverse T1-weighted), the large lesion enhances intensely, especially in the periphery during the arterial phase **(c). d:** In the portal venous phase the lesion is homogeneously hyperintense. The two smaller lesions do not show contrast enhancement (cysts). **e:** GRE transverse T1-weighted images obtained 2 hours after administration of Gd-BOPTA. The large lesion is hypointense because of lack of persistent contrast media (CM) uptake. The gallbladder is markedly hyperintense due to CM in the bile.

tions (143) decrease signal intensity on T2-weighted images (Fig. 19a).

AU5 The presence of a peripheral hyperintense halo, more AU6 than to edema, seems to have contribution srom edema as well as marginal infiltration into adjacent liver with zones of necrosis (142). In about 25% of colorectal hepatic metastases a hypointense peripheral rim is observed in the parenchyma around tumor nodules on T2-weighted images. The associated histopathologic changes are compression of hepatic parenchyma, hepatocellular atrophy, fibrosis, inflammation, and congested sinusoids (142).

In some cases, the production of paramagnetic substances modifies the appearance of metastases on T1-weighted images. The melanin present in the metastases from melanoma increases the signal intensity on T1-weighted images. The mucin (in metastases from macrocystic adenocarcinoma of the pancreas or ovary) increases the signal intensity on T1-weighted images because of the binding of water molecules with proteinaceous macromolecules, thus reducing the content of free water molecules (140).

Dynamic MRI with ECF agents has been shown to be equivalent to spiral CTAP for lesion detection in one study (144). On hepatic arterial phase, metastases can show a fleeting ring enhancement that blurs the margins of the lesions and corresponds to a desmoplastic reaction, inflammatory infiltration, and vascular proliferation in the tumor liver parenchyma margin (Fig. 19c). Enhancement progresses centrally with concomitant peripheral washout (Fig. 18). In the equilibrium phase (10 minutes after administration of contrast material), some lesions show a peripheral hypointense rim ("peripheral washout" sign; Fig. 18d). Mafhouz et al. (134) reported that this sign was absent in all of the benign lesions ($p < 0.001$), with a sensitivity of 24.5% and a specificity of 100% in the diagnosis of malignancies of the liver.

After Gd-BOPTA administration, the dynamic study is superimposable with that obtained with conventional extravascular-extracellular Gd-based contrast agents. In the hepatobiliary, phase the lesions do not show significant enhancement because they cannot uptake the CM (3). When there is a desmoplastic reaction to the lesion, an accumulation in the fibrotic part can be observed, which can remain for several hours. In these cases, observation

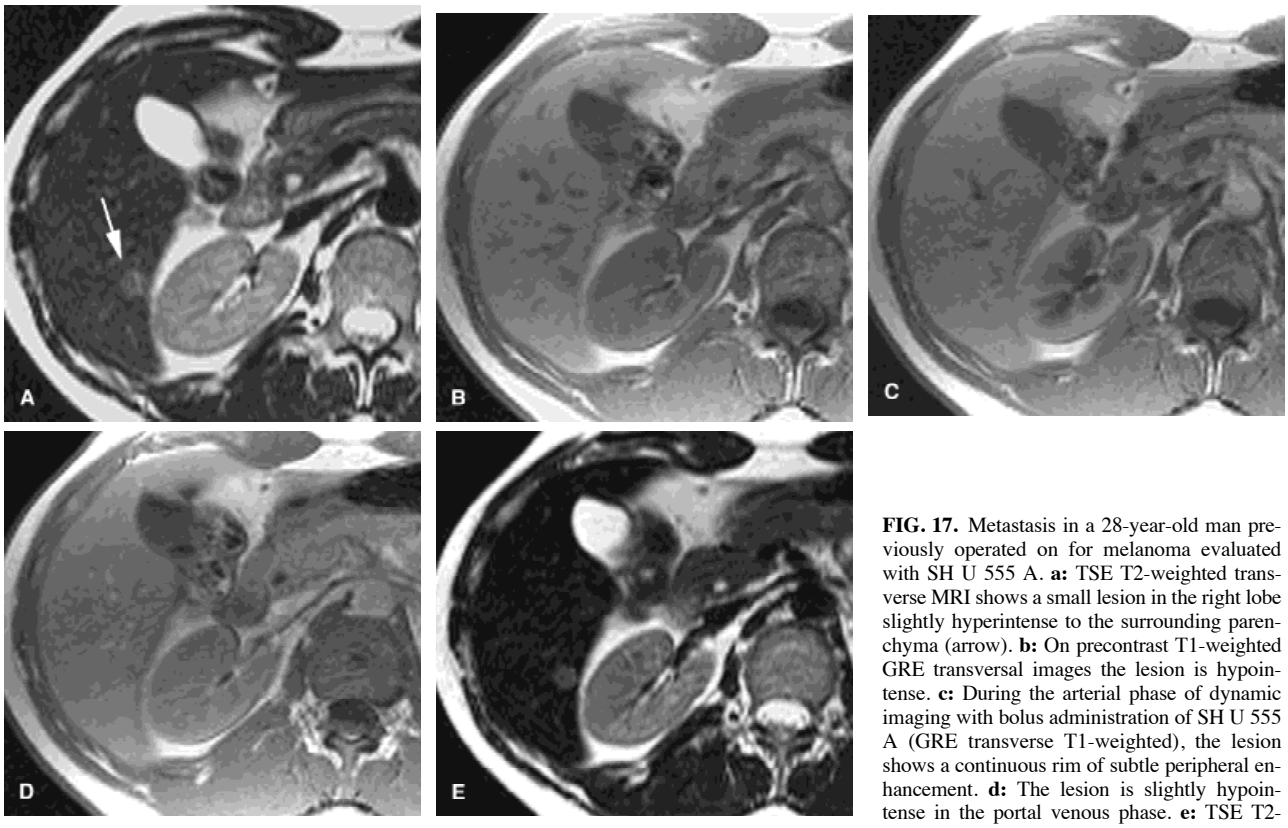


**FIG. 17.** Metastasis in a 28-year-old man previously operated on for melanoma evaluated with SH U 555 A. **a:** TSE T2-weighted transverse MRI shows a small lesion in the right lobe slightly hyperintense to the surrounding parenchyma (arrow). **b:** On precontrast T1-weighted GRE transversal images the lesion is hypointense. **c:** During the arterial phase of dynamic imaging with bolus administration of SH U 555 A (GRE transverse T1-weighted), the lesion shows a continuous rim of subtle peripheral enhancement. **d:** The lesion is slightly hypointense in the portal venous phase. **e:** TSE T2-weighted transverse MRI 10 minutes after SH U 555 A injection. Slight homogeneous signal drop is observed throughout the liver parenchyma. The lesion shows a lack of contrast media uptake; thus, it appears more hyperintense to the surrounding liver parenchyma.

of a peripheral hypointense halo of the lesion is highly suggestive of the malignant nature of the lesion (Fig. 19e and f).

After injection of Gd-EOB-DTPA, liver metastases demonstrated inhomogeneous uptake of Gd-EOB-DTPA during the distribution phase, with a washout effect on delayed images at 3 minutes and the highest tumor liver contrast seen at 20 and 45 minutes after contrast (145). After Mn-DPDP there is an increase of the liver-to-lesion CNR because of the lack of contrast uptake.

Colorectal metastases show a rim enhancement (Fig. 19g) that is generally more pronounced on more delayed (24 hours after injection) images compared with images obtained 1 hour after infusion. This rim has been postulated to be due to the compression of peritumoral sinusoidal spaces, with poor excretion of contrast agent and hence early and delayed enhancement (116).

Metastases do not contain RES cells; thus. after SPIO injection the liver metastasis CNR is improved with increased lesion conspicuity and detection compared with F20 nonenhanced T2-weigted images (Fig. 20) (45,146, 147).

Because of the nonspecific behavior of malignant liver lesions after SPIO injection, some authors have proposed a dual contrast study to improve lesion characterization. Pre-SPIO and post-SPIO injection images are obtained, followed by bolus injection of Gd-DTPA and multiphasic dynamic T1-weighted GRE images (124,148,149).

After injection of SPIO the quality of Gd-enhanced sequences is not diminished, and the same features observed in conventional (ECF-only) dynamic studies for a variety of lesions are valid for characterization purposes. In particular, metastases showed rim enhancement on the earlier images with a delayed central enhancement in almost all lesions, whereas peripheral washout was observed in about one third of the lesions (122).

With USPIO a hyperintense rim enhancement noted in some patients may be due to blood pool enhancement in peripheral vessels surrounding malignant tissue observed on T1-weighted images (54). This finding may constitute an additional feature for characterization of metastases. Moreover, the persistence of a T1 blood pool effect of AMI-25 has implications for tumor differentiation between hemangiomas (which present blood pool effect) and

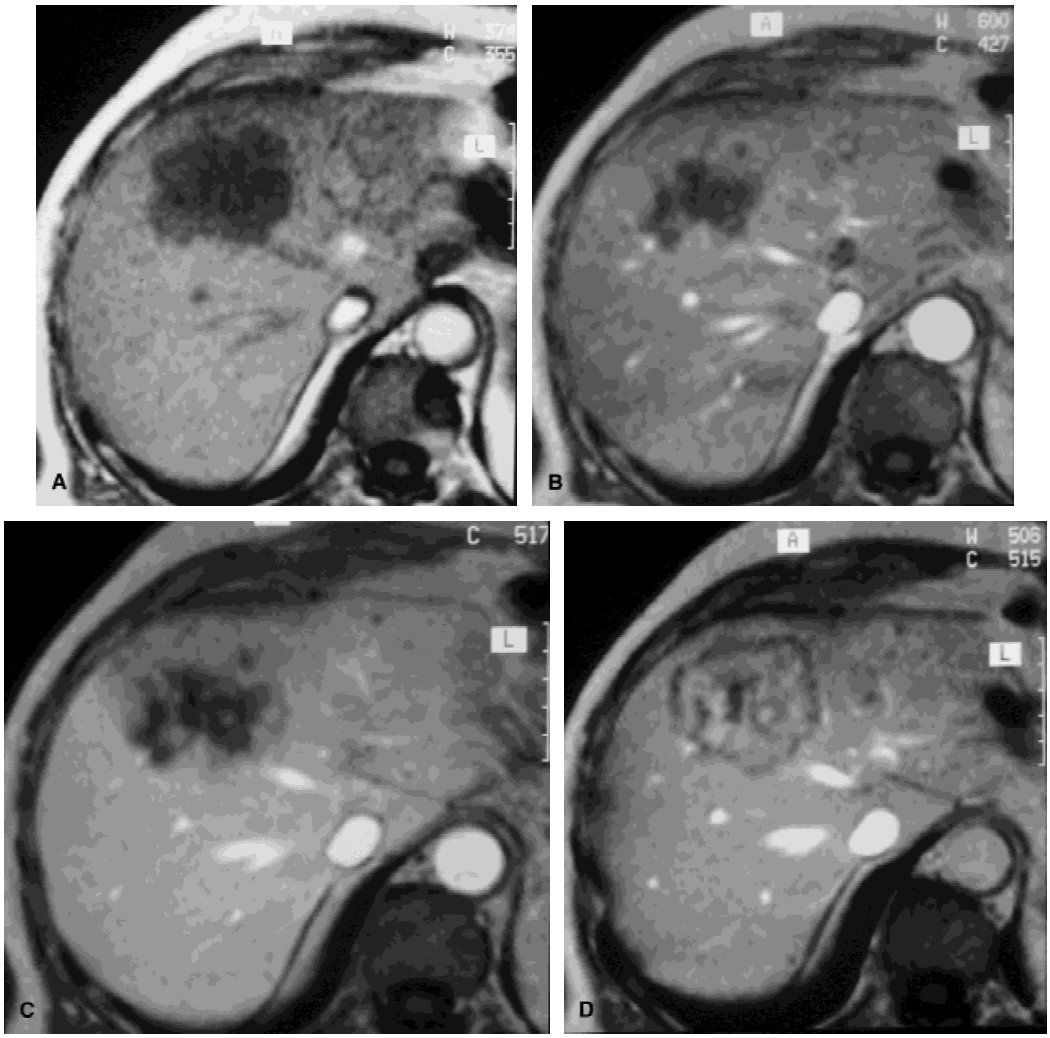


**FIG. 18.** Metastasis in a patient previously operated on for colon carcinoma with dynamic administration of Gd-BOPTA showing peripheral washout. **a:** GRE transverse T1 precontrast image. Large lesion with cauliflower aspect is homogeneously hypointense. **b:** During the arterial phase with bolus administration of Gd-BOPTA (GRE transverse T1-weighted), the large lesion at shows a fleeting ring enhancement that blurs the margins of the lesions. **c:** In the portal venous phase the enhancement progresses centrally. **d:** At the equilibrium phase a peripheral hypointense rim ("peripheral washout" sign) can be seen.

metastases, when T1-weighted gradient-echo images are performed (150).

### Focal liver lesions with delayed persistent enhancement

In this section the focal liver lesions in which enhancement is more evident during the late phase of dynamic study are described. The most frequent lesions encountered in this group are hemangiomas and cholangiocarcinomas.

*Hemangiomas* are the most common benign tumors of the liver, with a reported incidence ranging from 1% to 20%. Hemangiomas occur more commonly in women (female/male ratio 5:1). Although hemangiomas may be present on patients of all ages, they are seen more commonly in premenopausal women (151,152). The hemangioma usually is well circumscribed and blood filled. It ranges in size from a few millimeters to more than 20 cm. Hemangiomas larger than 10 cm are designated as giant hemangiomas (153). Hemangiomas may occur in conjunction with FNH (15%–20%). It frequently is a solitary tumor, although multiple hemangiomas occur in about 10% to 20% of cases (154).

On cut sections, hemangiomas almost always are heterogeneous with areas of fibrosis, necrosis. and cystic change Sometimes abundant fibrous tissue completely replaces the lesion. Calcification is rare in this tumor (less than 10%) and can be either large and coarse, with phlebolith-like thrombi within the vascular channels of the hem-

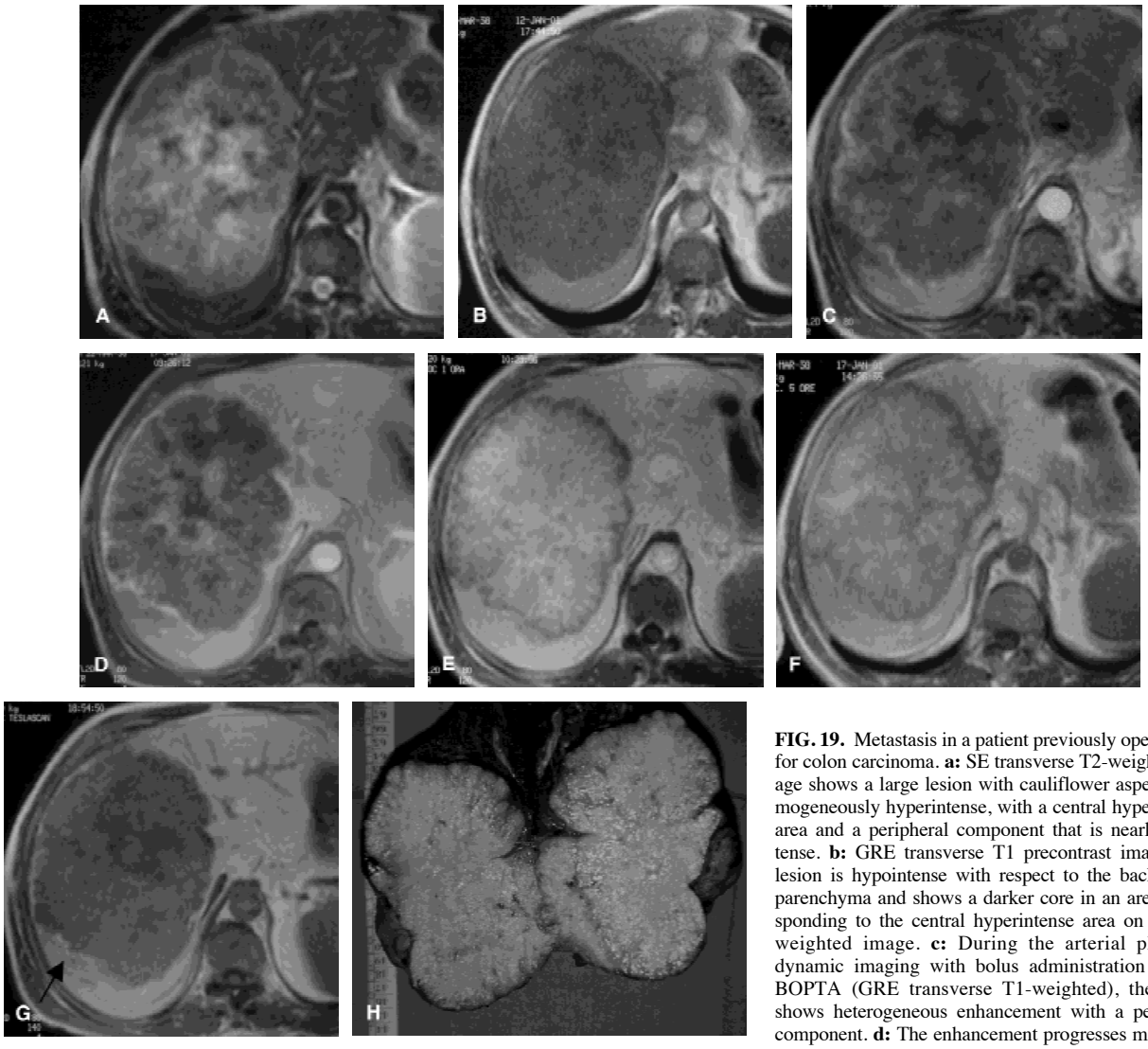


**FIG. 19.** Metastasis in a patient previously operated on for colon carcinoma. **a:** SE transverse T2-weighted image shows a large lesion with cauliflower aspect inhomogeneously hyperintense, with a central hyperintense area and a peripheral component that is nearly isointense. **b:** GRE transverse T1 precontrast image. The lesion is hypointense with respect to the background parenchyma and shows a darker core in an area corresponding to the central hyperintense area on the T2-weighted image. **c:** During the arterial phase of dynamic imaging with bolus administration of Gd-BOPTA (GRE transverse T1-weighted), the lesion shows heterogeneous enhancement with a peripheral component. **d:** The enhancement progresses more centrally in the portal venous phase. **e:** In the hepatobiliary phase 1 hour after injection of Gd-BOPTA, the lesion shows substantial but heterogeneous enhancement due to accumulation of contrast media (CM) in the fibrotic area. **f:** The enhancement still can be seen 5 hours after CM injection. **g:** GRE transverse T1-weighted image 1 hour after Mn-DPDP injection. The lesion is markedly hypointense due to lack of contrast uptake. A peripheral rim enhancement can be observed (arrow). **h:** Surgical specimen from a segmental resection shown for correlation.

angioma (131,151). Microscopically it is composed of multiple vascular channels lined by a single layer of endothelial cells supported by a thin fibrous stroma.

Hemangiomas usually are asymptomatic, and results of liver function tests are normal. Rarely patients present with abdominal pain. Exceptionally the clinical picture is an inflammatory syndrome of fever and leukocytosis or thrombocytopenia and fibrinopenia or cholestasis without jaundice. These atypical presentations sometimes are associated with intratumoral hemorrhage or thrombosis; spontaneous rupture is distinctly rare (131). Asymptomatic hemangiomas should not be treated. Most hemangiomas can be managed conservatively.

Hepatic resection for cavernous hemangioma should be performed only in patients with moderate-to-severe symptoms, complicated lesions, or both, because most benign lesions have a good natural course. Less invasive surgical procedures are being recommended with increasing frequency for cases in which treatment of these benign tumors is indicated (152,155).

On MRI, hemangiomas characteristically demonstrate marked hyperintensity on T2-weighted images (Figs. 3a and 21a), which may contain low-intensity areas that correlate with zones of fibrosis (Fig. 22a) (156). On precontrast T1-weighted images, hemangioma is seen most commonly as a well-defined slightly hypointense mass with

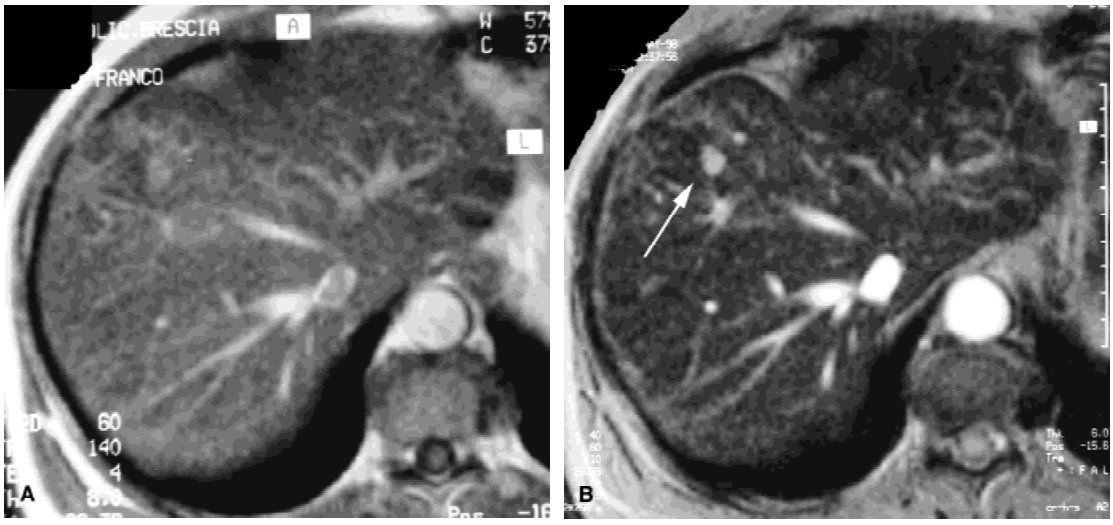


**FIG. 20.** Metastasis in a 55-year-old man previously operated on for colon carcinoma. FLASH T2*-weighted transverse image before **(a)** and after 1 hour after **(b)** Endorem administration. **a:** On unenhanced imaging a subtle, slight hyperintense lesion can be seen in the right lobe. **b:** After Endorem administration a marked signal drop in the liver parenchyma can be seen, rendering the lesion clearly visible (arrow).

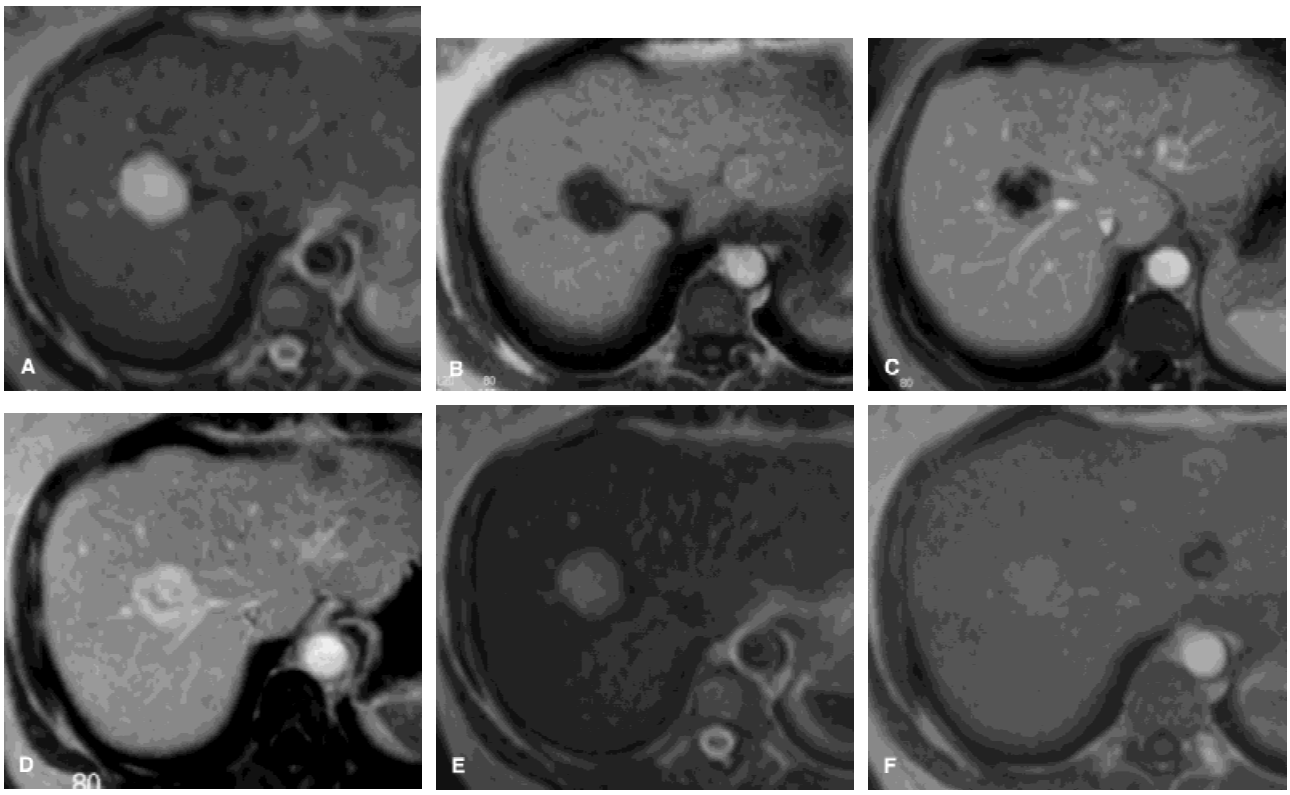


**FIG. 21.** Hemangioma in a 53-year-old woman. **a:** SE transverse T2-weighted image shows a round hyperintense lesion in the right lobe of the liver, which is hypointense on GRE transverse T1 precontrast image **(b).** During dynamic imaging with bolus administration of Gd-BOPTA (GRE transverse T1-weighted), the lesion shows a globular peripheral enhancement, starting in the arterial phase **(c)** and becoming homogeneously hyperintense on the distribution phase **(d). e:** SE transverse T2-weighted images 1 hour after administration of Endorem. Homogeneous signal drop is observed throughout the liver and the lesion, which persists slightly hyperintense to the surrounding liver parenchyma. **f:** GRE transverse T1-weighted image 1 hour after administration of Endorem. The hemangioma appears slightly hyperintense.

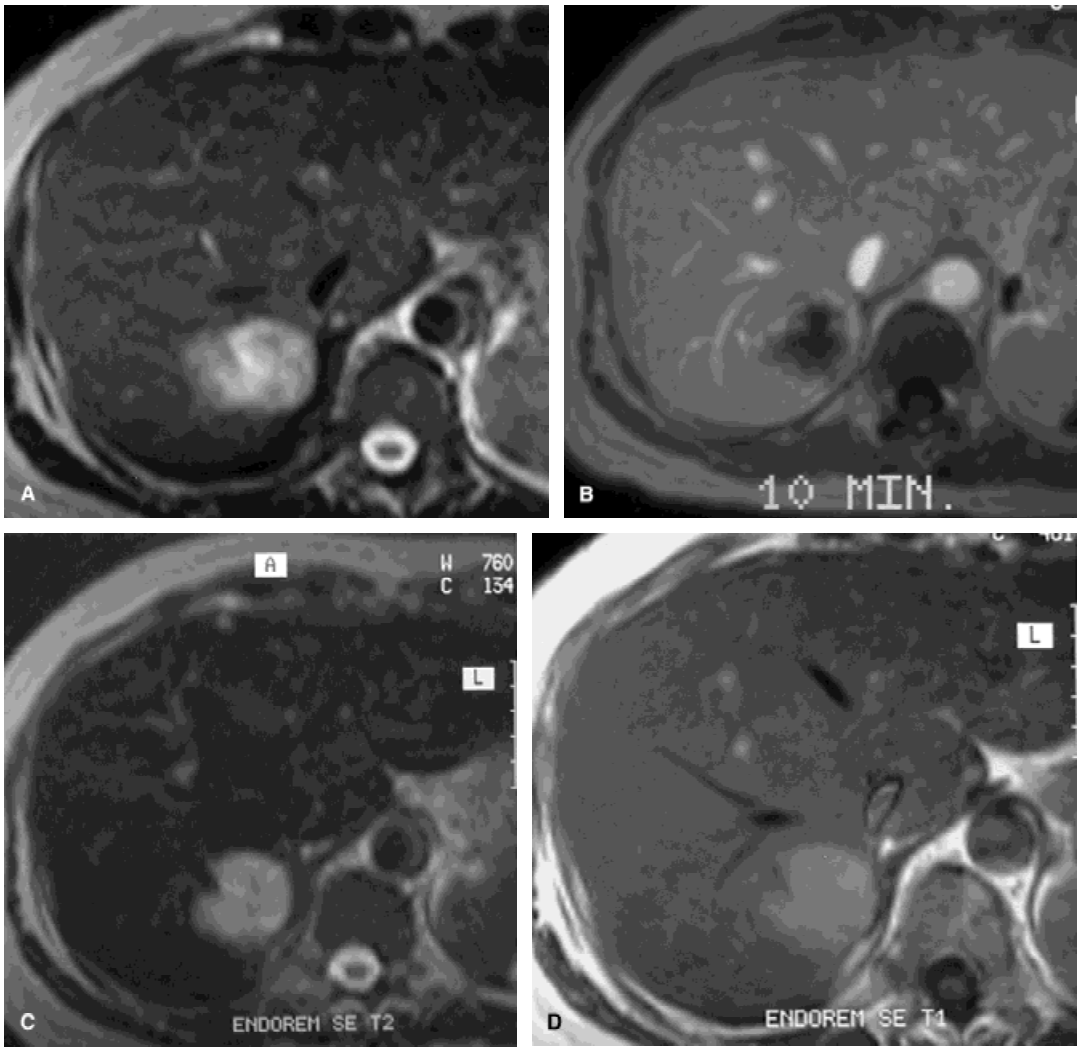


**FIG. 22.** Atypical hemangioma in a 45-year-old man previously operated on for colon carcinoma. **a:** SE transverse T2-weighted image shows an inhomogeneously hyperintense lesion in the right lobe of the liver. During dynamic imaging with bolus administration of Gd-BOPTA (GRE transverse T1-weighted), the lesion shows a peripheral enhancement, which does not reach the center of the lesion until the distribution phase **(b)** and then only with slight enhancement. **c:** SE transverse T2-weighted images 1 hour after administration of Endorem. Homogeneous signal drop throughout the liver and the lesion. **d:** SE transverse T1-weighted image 1 hour after administration of Endorem. The hemangioma appears slightly but uniformly hyperintense.

lobulated borders. The pattern of "nodular" enhancement after Gd injection was seen as highly specific for hemangioma (Fig. 21) compared with rim enhancement noted in metastases (156,157).

Three enhancement patterns of hemangioma with Gd-enhanced gradient-echo imaging have been noted: (1) immediate and complete enhancement of small lesions (so-called capillary hemangiomas; Fig. 14); (2) peripheral nodular enhancement progressing centripetally to uniform enhancement (Fig. 21d); and (3) peripheral nodular enhancement with persistent central hypointensity (Fig. 22b) (158). Uniform enhancement throughout the lesion on delayed images should not be used as a criterion for diagnosis because this will only lower the specificity (159). In the majority of cases the combination of T2-weighted and serial dynamic Gd images allows a confident diagnosis of hemangiomas (156).

On delayed liver-specific phase, after Gd-BOPTA or Mn-DPDP hemangiomas tend to be hypointense compared with the surrounding liver parenchyma (3,18). After SPIO injection, hemangiomas often lose signal on T2-weighted images (Figs. 3g, 21e, and 22c), whereas a significant increase of signal intensity has been reported on postcontrast T1-weighted images due to R1 relaxivity of low concentrated SPIO in vascular spaces of the hemangioma (Figs. 3h, 21f, and 22d) (48). Within hemangiomas the SPIO concentration is similar to that of vessels because of the high blood content of this tumor. Uptake of

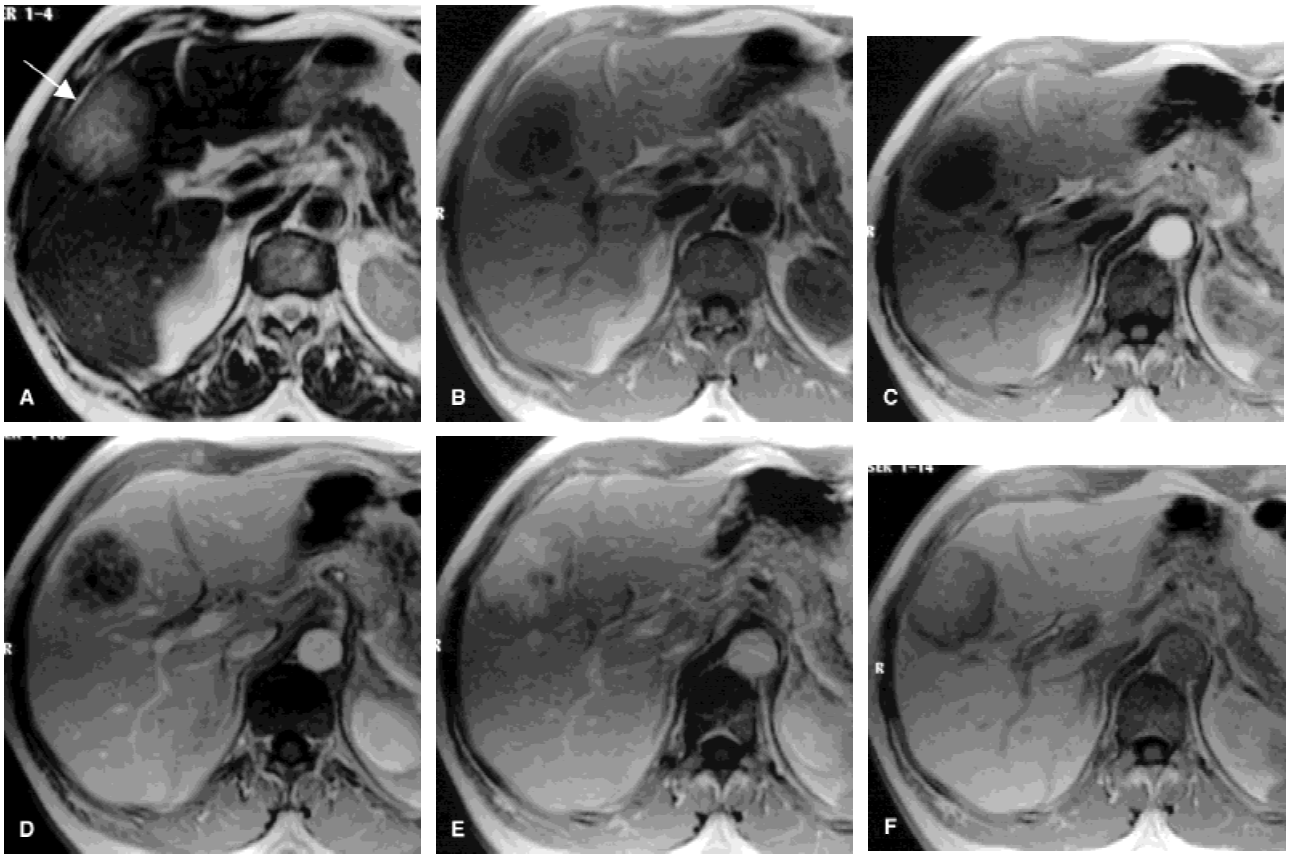


**FIG. 23.** Peripheral cholangiocarcinoma in a 70-year-old man. **a:** TSE transverse T2-weighted image shows a large heterogeneous, slightly hyperintense lesion with blurred margins in the right lobe of the liver and capsular retraction (arrow). **b:** GRE transverse T1 precontrast image. The lesion is homogeneously hypointense to the surrounding liver parenchyma. **c:** During the arterial phase of dynamic imaging with bolus administration of Gd-BOPTA (GRE transverse T1-weighted), the lesion is homogeneously hypointense. **d:** In the portal venous phase, the lesion shows some enhancement with a lace-like pattern. **e:** In the distribution phase, the enhancement has become clearly evident. **f:** GRE transverse T1-weighted images obtained 2 hours after administration of Gd-BOPTA. Homogeneous enhancement of the liver is noted. The lesion shows accumulation of contrast media in the desmoplastic area, with a peripheral zone of washout.

SPIO in hemangioma appears to be due to pooling of the contrast agent within the vascular channels of hemangiomas (83). With SHU 555 A it is possible to obtain both dynamic and RES phase imaging of hemangioma. Dynamic imaging shows the same morphologic features observed with Gd-enhanced dynamic MRI, whereas RES phase shows both T1 and T2 effect of SPIO.

*Cholangiocellular carcinoma* (CCC) is a malignant hepatic tumor of the biliary epithelium and is the second most common form of primary hepatic malignancy in adults after HCC (57). It represents less than 1% of all newly diagnosed cancers in North America and usually is seen in the seventh decade of life with a slight male predominance (160).

Several factors have been linked etiologically to the development of CCC, although none of the factors is evident in many patients. Cholangiocarcinoma is associated with clonorchiasis, intrahepatic stone disease, choledochal cyst, Caroli disease, and primary sclerosing cholangitis (161). Most of these risk factors have in common longstanding inflammation and injury to bile duct epithelium. Primary sclerosing cholangitis (PSC) is commonly associated with CCC, with as many as 10% of patients with PSC going on to develop CCC (162). This form of cancer sometimes occurs in the presence of cirrhosis and has been weakly correlated to hepatis C virus infection. Mixed AU7 hepato-cholangiocellular carcinomas have been described (163).

Cholangiocarcinoma usually is divided into "intrahepatic" and "extrahepatic," depending on the site of origin. For the purposes of this discussion only the intrahepatic subgroup is presented.

Intrahepatic cholangiocarcinoma (ICC) is a malignant neoplasm arising from the epithelium of the intrahepatic bile ducts and represents 10% of all cholangiocarcinomas. Hilar (Klatskin) and bile duct cholangiocarcinomas account for the remaining 90% (57). This neoplasm usually is a large firm mass. In 10% to 20% of cases there are

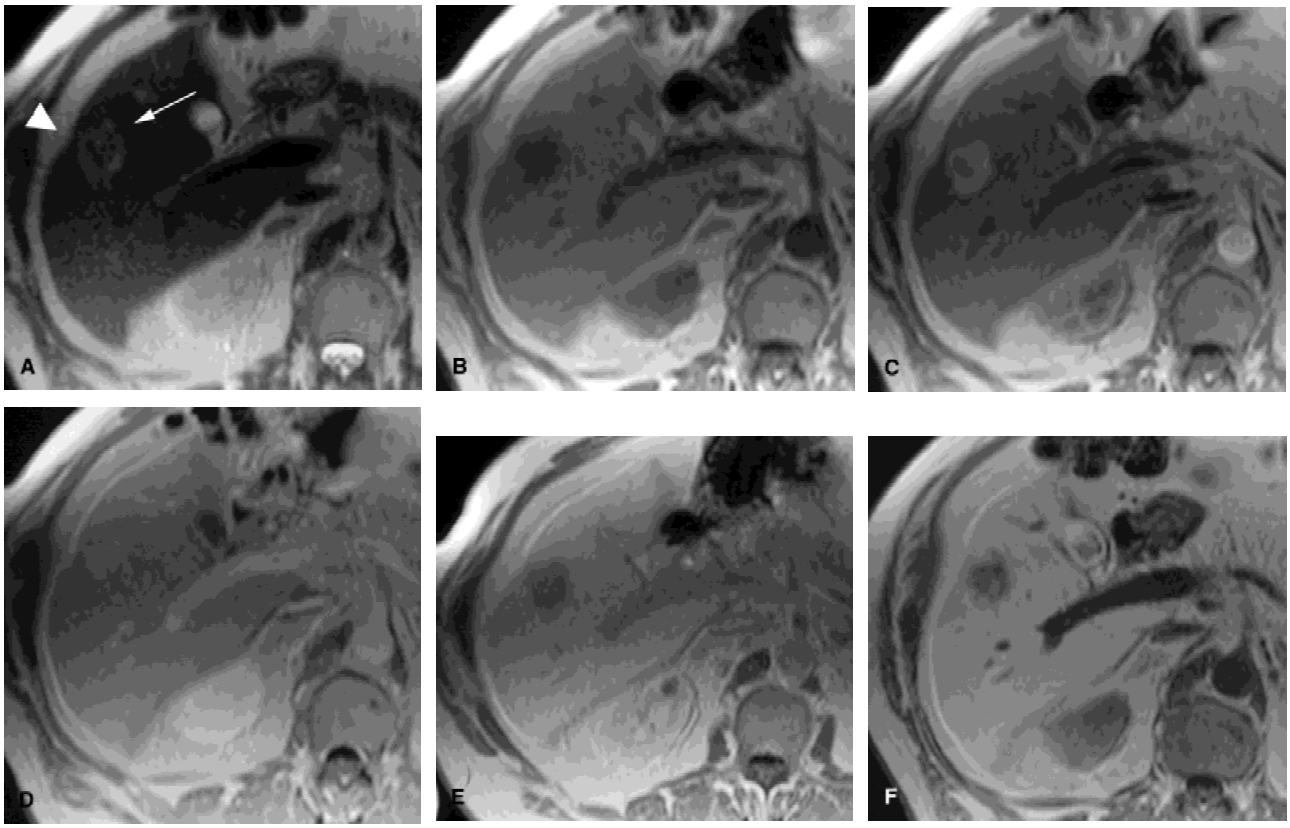


**FIG. 24.** Hypervascular peripheral cholangiocarcinoma in a 66-year-old man. **a:** HASTE transverse T2-weighted image shows a small isointense lesion with hyperintense margins in the right lobe of the liver (arrow) and capsular retraction (arrowhead). **b:** GRE transverse T1 precontrast image. The lesion is homogeneously hypointense to the surrounding liver parenchyma. **c:** During the arterial phase of dynamic imaging with bolus administration of Gd-BOPTA (GRE transverse T1-weighted), the lesion is hyperintense. **d:** In the portal venous phase, the lesion shows a persistent enhancement. **e:** GRE transverse T1-weighted images obtained 2 hours after administration of Gd-BOPTA. Homogeneous enhancement of the liver is evident, and the lesion is hypointense with slight accumulation of contrast media (CM) in the desmoplastic center. **f:** GRE transverse T1-weighted images obtained 1 hour after administration of Mn-DPDP. The lesion is hypointense with slight accumulation of CM in the desmoplastic area.

several satellite nodules around the main mass. On cut section, it is characterized by the presence of large amounts of whitish fibrous tissue. A variable amount of central necrosis could be present within the tumor, especially if it is large. Hemorrhage is rare (164).

Microscopically the tumor is an adenocarcinoma with a glandular appearance and cells resembling biliary epithelium. Mucin and calcification sometimes can be demonstrated. A large desmoplastic reaction is typical of cholangiocarcinoma. The liver parenchyma and hepatoduodenal ligaments commonly are invaded by Klatskin tumor. Lymphatic metastases most commonly involve the portocaval superior and posterior pancreaticoduodenal lymph nodes (165).

Clinical signs and symptoms are related to the site of origin of the tumor. In ICC, symptoms usually are vague until the tumor stage is far advanced and patients present with abdominal pain and a palpable mass in the upper abdomen. Jaundice is rarely a presenting symptom in ICC, whereas it is common with hilar or ductal cholangiocarcinoma (165,166). ICC is a relatively uncommon tumor with an insidious onset and late presentation contributing to poor survival. Surgical resection is the only therapeutic option. Because few patients are potentially resectable at the time of presentation, efforts at early diagnosis and options for adjuvant therapy are imperative. In selected patients, complete surgical resection can be performed safely and is associated with long-term survival. Surgical resection provides the best survival with a good quality of life for patients with hilar cholangiocarcinoma. Long-term survival after resection is significantly associated with less advanced tumor stages (165).

On MRI, ICC has a nonspecific appearance. It is isointense to hypointense on precontrast T1-weighted images. On T2-weighted images the signal intensity of the tumor ranges from markedly increased to mildly increased, relative to liver (Fig. 23a and b). Tumors with high fibrous content tend to have lower signal intensity on T2-weighted images (164,167).

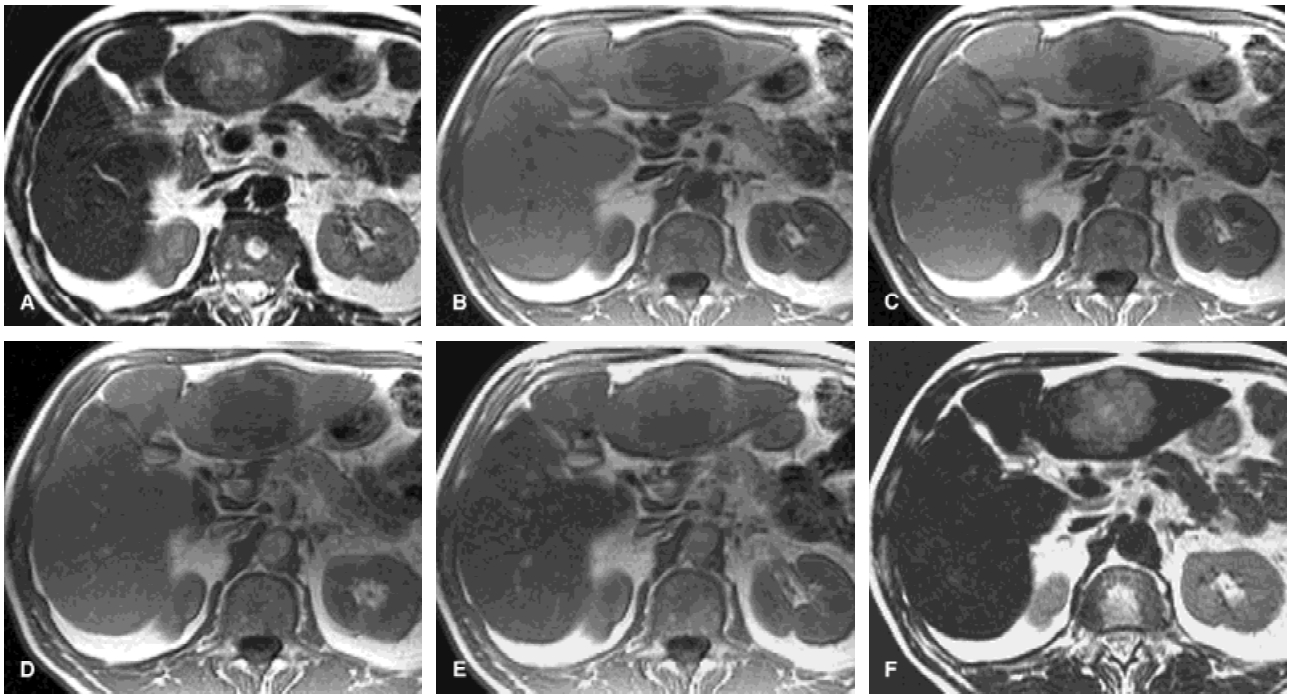


**FIG. 25.** Peripheral cholangiocarcinoma in a 62-year-old man. **a:** TSE transverse T2-weighted image shows a large hyperintense lesion in the left lobe of the liver. **b:** GRE transverse T1 precontrast image. The lesion is homogeneously hypointense to the surrounding liver parenchyma. During dynamic imaging with bolus administration of SH U 555 A (GRE transverse T1-weighted), the lesion does not show any significant enhancement in the arterial **(c)** and portal venous phases **(d). e:** GRE transverse T1-weighted images obtained 10 minutes after administration of SH U 555 A. Slight enhancement ED2 of the liver parenchyma at the margins of the lesion is seen. **e:** TSE transverse T2-weighted images obtained 10 minutes after administration of SH U 555 A. Homogenous signal drop of the liver parenchyma augments the contrast between the liver and the lesion.

With serial dynamic ECF-Gd enhanced images, cholangiocarcinomas show minimal or moderate incomplete rim of enhancement at the tumor periphery on early images, with progressive central contrast enhancement on later images (168). As with CT, contrast enhancement may be seen better on delayed images because of the nature of the tumor (Fig. 23c–e) (169).

Dynamic imaging with Gd-BOPTA is similar to nonspecific vasculo-interstitial Gd-based contrast agents, but in the hepato-biliary phase the lesion shows contrast en- F23 hancement in the fibrotic area (Fig. 23f). The degree of enhancement depends on the type of cholangiocarcinoma. Greater peripheral enhancement is noted in the early phases in large cholangiocarcinoma, whereas greater delayed enhancement is noted in the fibrous core of the "scirrhous" cholangiocarcinomas in the hepatobiliary phase (3). Occasionally some small peripheral cholangiocarcinomas with a large number of tumor cells and few interstitial fibrous tissues at dynamic magnetic resonance images reveal strong enhancement of the whole tumor on F24 the early phase (Fig. 24) (167), thus making difficult differentiation from other hypervascular hepatic tumors. Prolonged enhancement of the tumor on late and delayed phases of dynamic images could be of diagnostic value (170).

After Mn-DPDP administration no significant uptake is observed within the lesion (Fig. 24), although some peripheral rim enhancement has been observed (116), which has been attributed to peritumoral malignant infiltration and compression of surrounding normal liver tissue (117). The hepatobiliary phase after liver-specific CM adds useful information for identification of small satellite lesions. Analogously, after SPIO administration, because of the absence of Kupffer cells within the lesion, no significant uptake is observed, and there is an increase of liver-to-lesion contrast noise signal on T2-weighted images (Fig. 25) (171). F25

## CONCLUSION

Use of ECF Gd-based contrast agents with dynamic acquisitions is the predominant means of performing contrast-enhanced liver MRI. However, increased use of targeted CM can improve the sensitivity and specificity of MR study in the identification and characterization of focal liver lesions. As experience is gained with these

agents, new patterns of enhancement will be recognized and new combinations of imaging strategies will emerge. It is predicted that expertise with all of these agents will further reduce the need for tissue sampling and allow a better noninvasive means to triage patients with hepatic malignancies.

## REFERENCES


1. Hamm B, Thoeni RF, Gould RG, et al. Focal liver lesions: Characterization with nonenhanced and dynamic contrast material-enhanced MR imaging. Radiology 1994;190:417–423.
2. Grebe P, Schild H, Kreitner KF, et al. The differentiation between benign and malignant liver lesions by unenhanced MRI]. Rofo Fortschr Geb Rontgenstr Neuen Bildgeb Verfahr 1994;161:412–416. ED1
3. Petersein J, Spinazzi A, Giovagnoni A, et al. Focal liver lesions: Evaluation of the efficacy of gadobenate dimeglumine in MR imaging—A multicenter phase III clinical study. Radiology 2000; 215:727–736.
4. Hamm B, Fischer E, Taupitz M. Differentiation of hepatic hemangiomas from metastases by dynamic contrast-enhanced MR imaging. J Comput Assist Tomogr 1990;14:205–216.
5. Semelka RC, Shoenut JP, Kroeker MA, et al. Focal liver disease: Comparison of dynamic contrast-enhanced CT and T2-weighted fat-suppressed, FLASH, and dynamic gadolinium-enhanced MR imaging at 1.5 T. Radiology 1992;184:687–694.
6. Vogl TJ, Stupavsky A, Pegios W, et al. Hepatocellular carcinoma: Evaluation with dynamic and static gadobenate dimeglumine-enhanced MR imaging and histopathologic correlation. Radiology 1997;205:721–728.
7. Weinmann HJ, Laniado M, Mutzel W. Pharmacokinetics of GdDTPA/dimeglumine after intravenous injection into healthy volunteers. Physiol Chem Phys Med NMR 1984;16:167–172.
8. Kuwatsuru R, Kadoya M, Ohtomo K, et al. Comparison of gadobenate dimeglumine with gadopentetate dimeglumine for magnetic resonance imaging of liver tumors. Invest Radiol 2001;36:632–641.
9. Nakayama M, Yamashita Y, Mitsuzaki K, et al. Improved tissue characterization of focal liver lesions with ferumoxide-enhanced T1 and T2-weighted MR imaging. J Magn Reson Imaging 2000; 11:647–654.
10. Liou J, Lee JK, Borrello JA, et al. Differentiation of hepatomas from nonhepatomatous masses: Use of MnDPDP-enhanced MR images. Magn Reson Imaging 1994;12:71–79.
11. Vogl TJ, Kummel S, Hammerstingl R, et al. Liver tumors: Comparison of MR imaging with Gd-EOB-DTPA and Gd-DTPA. Radiology 1996;200:59–67.
12. Martin DR, Semelka RC, Chung JJ, et al. Sequential use of gadolinium chelate and mangafodipir trisodium for the assessment of focal liver lesions: Initial observations. Magn Reson Imaging 2000; 18:955–963.
13. Lim KO, Stark DD, Leese PT, et al. Hepatobiliary MR imaging: First human experience with MnDPDP. Radiology 1991;178: 79–82.
14. Rummeny EJ, Torres CG, Kurdziel JC, et al. MnDPDP for MR imaging of the liver. Results of an independent image evaluation of the European phase III studies. Acta Radiol 1997;38(4 pt 2):638–642.
15. Wang C. Mangafodipir trisodium (MnDPDP)-enhanced magnetic resonance imaging of the liver and pancreas. Acta Radiol Suppl 1998;415:1–31.
16. Mathieu D, Coffin C, Kobeiter H, et al. Unexpected MR-T1 enhancement of endocrine liver metastases with mangafodipir. J Magn Reson Imaging 1999;10:193–195.
17. Murakami T, Baron RL, Peterson MS, et al. Hepatocellular carcinoma: MR imaging with mangafodipir trisodium (Mn-DPDP). Radiology 1996;200:69–77.
18. Oudkerk M, Torres CG, Song B, et al. Characterization of liver lesions with mangafodipir trisodium-enhanced MR imaging: Multicenter study comparing MR and dual-phase spiral CT. Radiology 2002; (in press). AU8
19. Rofsky NM, Weinreb JC, Bernardino ME, et al. Hepatocellular tumors: Characterization with Mn-DPDP-enhanced MR imaging. Radiology 1993;188:53–59.
20. Coffin CM, Diche T, Mahfouz A, et al. Benign and malignant hepatocellular tumors: Evaluation of tumoral enhancement after mangafodipir trisodium injection on MR imaging. Eur Radiol 1999;9:444–449.
21. Kirchin MA, Pirovano GP, Spinazzi A. Gadobenate dimeglumine (Gd-BOPTA). An overview. Invest Radiol 1998;33:798–809.
22. Cavagna FM, Maggioni F, Castelli PM, et al. Gadolinium chelates with weak binding to serum proteins. A new class of high-efficiency, general purpose contrast agents for magnetic resonance imaging. Invest Radiol 1997;32:780–796.
23. Spinazzi A, Lorusso V, Pirovano G, et al. Safety, tolerance, biodistribution, and MR imaging enhancement of the liver with gadobenate dimeglumine: Results of clinical pharmacologic and pilot imaging studies in nonpatient and patient volunteers. Acad Radiol 1999;6:282–291.
24. Spinazzi A, Lorusso V, Pirovano G, et al. Multihance clinical pharmacology: Biodistribution and MR enhancement of the liver. Acad Radiol 1998;5(suppl 1):S86–S89, discussion S93–S84.
25. Grazioli L, Kirchin M, Pirovano G, et al. MultiHance in the dynamic phase of contrast enhancement: A pictorial assessment. J Comput Assist Tomogr 1999;239(suppl 1):S61–S64.
26. Caudana R, Morana G, Pirovano GP, et al. Focal malignant hepatic lesions: MR imaging enhanced with gadolinium benzyloxypropionictetra-acetate (BOPTA)—Preliminary results of phase II clinical application. Radiology 1996;199:513–520.
27. Manfredi R, Maresca G, Baron RL, et al. Delayed MR imaging of hepatocellular carcinoma enhanced by gadobenate dimeglumine (Gd-BOPTA). J Magn Reson Imaging 1999;9:704–710.
28. Grazioli L, Morana G, Federle MP, et al. Focal nodular hyperplasia: Morphologic and functional information from MR imaging with gadobenate dimeglumine. Radiology 2001;221:731–739.
29. Schuhmann-Giampieri G. Liver contrast media for magnetic resonance imaging. Interrelations between pharmacokinetics and imaging. Invest Radiol 1993;28:753–761.
30. Hamm B, Staks T, Muhler A, et al. Phase I clinical evaluation of Gd-EOB-DTPA as a hepatobiliary MR contrast agent: Safety, pharmacokinetics, and MR imaging. Radiology 1995;195:785–792.
31. Enochs WS, Weissleder R. Organ-and-tissue directed MRI contrast agents. In: Edelman RR, Hesselink JR, Zlatkin MB, eds. Clinical Magnetic Resonance Imaging. Philadelphia: WB Saunders, 192–200. AU9
32. Fahlvik AK, Klaveness J, Stark DD. Iron oxides as MR imaging contrast agents. J Magn Reson Imaging 1993;3:187–194.
33. Weissleder R, Stark DD, Engelstad BL, et al. Superparamagnetic iron oxide: Pharmacokinetics and toxicity. AJR Am J Roentgenol 1989;152:167–173.
34. Yamashita Y, Yamamoto H, Hirai A, et al. MR imaging enhancement with superparamagnetic iron oxide in chronic liver disease: Influence of liver dysfunction and parenchymal pathology. Abdom Imaging 1996;21:318–323.
35. Josephson L, Lewis J, Jacobs P, et al. The effects of iron oxides on proton relaxivity. Magn Reson Imaging 1988;6:647–653.
36. Fretz CJ, Elizondo G, Weissleder R, et al. Superparamagnetic iron oxide-enhanced MR imaging: Pulse sequence optimization for detection of liver cancer. Radiology 1989;172:393–397.
37. Schwartz LH, Seltzer SE, Tempany CM, et al. Superparamagnetic iron oxide hepatic MR imaging: Efficacy and safety using conventional and fast spin-echo pulse sequences. J Magn Reson Imaging 1995;5:566–570.

38. Kanematsu M, Hoshi H, Murakami T, et al. Fat-suppressed T2-weighted MR imaging of hepatocellular carcinoma and metastases: Comparison of conventional spin-echo, fast spin-echo, and echo-planar pulse sequences. J Magn Reson Imaging 1999;10:25–32.
39. Alger JR, Harreld JH, Chen S, et al. Time-to-echo optimization for spin echo magnetic resonance imaging of liver metastasis using superparamagnetic iron oxide particles. J Magn Reson Imaging 2001;14:586–594.
40. Deckers F, Corthouts B, Nackaerts Y, et al. The influence of MR field strength on the detection of focal liver lesions with superparamagnetic iron oxide. Eur Radiol 1997;7:887–892.
41. Hahn PF, Saini S. Liver-specific MR imaging contrast agents. Radiol Clin North Am 1998;36:287–297.
42. Gandon Y, Heautot JF, Brunet F, et al. Superparamagnetic iron oxide: Clinical time-response study. Eur J Radiol 1991;12:195–200.
43. Ros PR, Freeny PC, Harms SE, et al. Hepatic MR imaging with ferumoxides: A multicenter clinical trial of the safety and efficacy in the detection of focal hepatic lesions. Radiology 1995;196:481–488.
44. Muller RD, Vogel K, Neumann K, et al. MRI with supermagnetic iron particles versus double-spiral CT in identification of malignant liver lesions. Rofo Fortschr Geb Rontgenstr Neuen Bildgeb Verfahr 1998;168:436–443.
45. Seneterre E, Taourel P, Bouvier Y, et al. Detection of hepatic metastases: Ferumoxides-enhanced MR imaging versus unenhanced MR imaging and CT during arterial portography. Radiology 1996;200:785–792.
46. Strotzer M, Gmeinwieser J, Schmidt J, et al. Diagnosis of liver metastases from colorectal adenocarcinoma. Comparison of spiral-CTAP combined with intravenous contrast-enhanced spiral-CT and SPIO-enhanced MR combined with plain MR imaging. Acta Radiol 1997;38:986–992.
47. Weissleder R. Liver MR imaging with iron oxides: Toward consensus and clinical practice. Radiology 1994;193:593–595.
48. Grangier C, Tourniaire J, Mentha G, et al. Enhancement of liver hemangiomas on T1-weighted MR SE images by superparamagnetic iron oxide particles. J Comput Assist Tomogr 1994;18:888–896.
49. Kopp AF, Laniado M, Dammann F, et al. MR imaging of the liver with Resovist: Safety, efficacy, and pharmacodynamic properties. Radiology 1997;204:749–756.
50. Kehagias DT, Gouliamos AD, Smyrniotis V, et al. Diagnostic efficacy and safety of MRI of the liver with superparamagnetic iron oxide particles (SH U 555 A). J Magn Reson Imaging 2001;14:595–601.
51. Reimer P, Jahnke N, Fiebich M, et al. Hepatic lesion detection and characterization: Value of nonenhanced MR imaging, superparamagnetic iron oxide-enhanced MR imaging, and spiral CT-ROC analysis. Radiology 2000;217:152–158.
52. Saini S, Edelman RR, Sharma P, et al. Blood-pool MR contrast material for detection and characterization of focal hepatic lesions: Initial clinical experience with ultrasmall superparamagnetic iron oxide (AMI-227). AJR Am J Roentgenol 1995;164:1147–1152.
53. Harisinghani MG, Saini S, Weissleder R, et al. Differentiation of liver hemangiomas from metastases and hepatocellular carcinoma at MR imaging enhanced with blood-pool contrast agent Code-7227. Radiology 1997;202:687–691.
54. Mergo PJ, Helmberger T, Nicolas AI, et al. Ring enhancement in ultrasmall superparamagnetic iron oxide MR imaging: A potential new sign for characterization of liver lesions. AJR Am J Roentgenol 1996;166:379–384.
55. Nguyen BN, Flejou JF, Terris B, et al. Focal nodular hyperplasia of the liver: A comprehensive pathologic study of 305 lesions and recognition of new histologic forms. Am J Surg Pathol 1999;23:1441–1454.
56. Benhamou JP. Oral contraceptives and benign tumors of the liver. Gastroenterol Clin Biol 1997;21:913–915.
57. Craig JR, Peters RL, Edmonson HA. Tumors of the Liver and Intrahepatic Bile Ducts: Atlas of Tumors Pathology. Washington, DC: Armed Forced Institute of Pathology, 1989.
58. Cherqui D, Rahmouni A, Charlotte F, et al. Management of focal nodular hyperplasia and hepatocellular adenoma in young women: A series of 41 patients with clinical, radiological, and pathological correlations. Hepatology 1995;22:1674–1681.
59. Mathieu D, Rahmouni A, Anglade MC, et al. Focal nodular hyperplasia of the liver: Assessment with contrast-enhanced Turbo-FLASH MR imaging. Radiology 1991;180:25–30.
60. Carlson SK, Johnson CD, Bender CE, et al. CT of focal nodular hyperplasia of the liver. AJR Am J Roentgenol 2000;174:705–712.
61. Arbab AS, Ichikawa T, Araki T, et al. Detection of hepatocellular carcinoma and its metastases with various pulse sequences using superparamagnetic iron oxide (SHU-555-A). Abdom Imaging 2000;25:151–158.
62. Choi CS, Freeny PC. Triphasic helical CT of hepatic focal nodular hyperplasia: Incidence of atypical findings. AJR Am J Roentgenol 1998;170:391–395.
63. Boulahdour H, Cherqui D, Charlotte F, et al. The hot spot hepatobiliary scan in focal nodular hyperplasia. J Nucl Med 1993;34:2105–2110.
64. Paley MR, Mergo PJ, Torres GM, et al. Characterization of focal hepatic lesions with ferumoxides-enhanced T2-weighted MR imaging. AJR Am J Roentgenol 2000;175:159–163.
65. Grandin C, Van Beers BE, Robert A, et al. Benign hepatocellular tumors: MRI after superparamagnetic iron oxide administration. J Comput Assist Tomogr 1995;19:412–418.
66. Grazioli L, Morana G, Caccia P, et al. MR imaging of FNH with Gd-BOPTA and SPIO: A comparison. In: ECR 2002. Vienna: Springer, 2002;283.
67. Wanless IR. Micronodular transformation (nodular regenerative hyperplasia) of the liver: A report of 64 cases among 2,500 autopsies and a new classification of benign hepatocellular nodules. Hepatology 1990;11:787–797.
68. Arvanitaki M, Adler M. Nodular regenerative hyperplasia of the liver. A review of 14 cases. Hepatogastroenterology 2001;48:1425–1429.
69. Rougier P, Degott C, Rueff B, et al. Nodular regenerative hyperplasia of the liver. Report of six cases and review of the literature. Gastroenterology 1978;75:169–172.
70. Casillas C, Marti-Bonmati L, Galant J. Pseudotumoral presentation of nodular regenerative hyperplasia of the liver: Imaging in five patients including MR imaging. Eur Radiol 1997;7:654–658.
71. Soe KL, Soe M, Gluud C. Liver pathology associated with the use of anabolic-androgenic steroids. Liver 1992;12:73–79.
72. Grazioli L, Federle MP, Brancatelli G, et al. Hepatic adenomas: Imaging and pathologic findings. Radiographics 2001;21:877–892, discussion 892–874.
73. Labrune P, Trioche P, Duvaltier I, et al. Hepatocellular adenomas in glycogen storage disease type I and III: A series of 43 patients and review of the literature. J Pediatr Gastroenterol Nutr 1997;24:276–279.
74. Talente GM, Coleman RA, Alter C, et al. Glycogen storage disease in adults. Ann Intern Med 1994;120:218–226.
75. Shuangshoti S, Thaicharoen A. Hepatocellular adenoma in a beta-thalassemic woman having secondary iron overload. J Med Assoc Thai 1994;77:108–112.
76. Rubin RA, Lichtenstein GR. Hepatic scintigraphy in the evaluation of solitary solid liver masses. J Nucl Med 1993;34:697–705.
77. Leese T, Farges O, Bismuth H. Liver cell adenomas. A 12-year surgical experience from a specialist hepato-biliary unit. Ann Surg 1988;208:558–564.
78. Nokes SR, Baker ME, Spritzer CE, et al. Hepatic adenoma: MR appearance mimicking focal nodular hyperplasia. J Comput Assist Tomogr 1988;12:885–887.
79. Gabata T, Matsui O, Kadoya M, et al. MR imaging of hepatic adenoma. AJR Am J Roentgenol 1990;155:1009–1011.
80. Paulson EK, McClellan JS, Washington K, et al. Hepatic adenoma:

MR characteristics and correlation with pathologic findings. AJR Am J Roentgenol 1994;163:113–116.
81. Arrive L, Flejou JF, Vilgrain V, et al. Hepatic adenoma: MR findings in 51 pathologically proved lesions. Radiology 1994;193:507–512.
82. Chung KY, Mayo-Smith WW, Saini S, et al. Hepatocellular adenoma: MR imaging features with pathologic correlation. AJR Am J Roentgenol 1995;165:303–308.
83. Denys A, Arrive L, Servois V, et al. Hepatic tumors: Detection and characterization at 1-T MR imaging enhanced with AMI-25. Radiology 1994;193:665–669.
84. Flejou JF, Barge J, Menu Y, et al. Liver adenomatosis. An entity distinct from liver adenoma? Gastroenterology 1985;89:1132–1138.
85. Ribeiro A, Burgart LJ, Nagorney DM, et al. Management of liver adenomatosis: Results with a conservative surgical approach. Liver Transplant Surg 1998;4:388–398.
86. Choi BI, Han JK, Kim SH, et al. MR findings in liver adenomatosis. Gastrointest Radiol 1991;16:234–236.
87. Khan SS, Fink M, King S. Case report: Liver adenomatosis presenting as multiple calcified masses. Clin Radiol 1992;45:206–207.
88. Grazioli L, Federle MP, Ichikawa T, et al. Liver adenomatosis: Clinical, histopathologic, and imaging findings in 15 patients. Radiology 2000;216:395–402.
89. Chiche L, Dao T, Salame E, et al. Liver adenomatosis: Reappraisal, diagnosis, and surgical management: Eight new cases and review of the literature. Ann Surg 2000;231:74–81.
90. Bruix J, Sherman M, Llovet JM, et al. Clinical management of hepatocellular carcinoma. Conclusions of the Barcelona-2000 EASL conference. European Association for the Study of the Liver. J Hepatol 2001;35:421–430.
91. Ince N, Wands JR. The increasing incidence of hepatocellular carcinoma. N Engl J Med 1999;340:798–799.
92. Zaman SN, Melia WM, Johnson RD, et al. Risk factors in development of hepatocellular carcinoma in cirrhosis: Prospective study of 613 patients. Lancet 1985;1:1357–1360.
93. Sadek AG, Mitchell DG, Siegelman ES, et al. Early hepatocellular carcinoma that develops within macroregenerative nodules: Growth rate depicted at serial MR imaging. Radiology 1995;195:753–756.
94. Rapaccini GL, Pompili M, Caturelli E, et al. Focal ultrasound lesions in liver cirrhosis diagnosed as regenerating nodules by fine-needle biopsy. follow up of 12 cases. Dig Dis Sci 1990;35:422–427.
95. Takayama T, Makuuchi M, Hirohashi S, et al. Malignant transformation of adenomatous hyperplasia to hepatocellular carcinoma. Lancet 1990;336:1150–1153.
96. Wanless IR. Terminology of nodular hepatocellular lesions. International Working Party. Hepatology 1995;22:983–993.
97. Krinsky GA, Lee VS, Theise ND, et al. Hepatocellular carcinoma and dysplastic nodules in patients with cirrhosis: Prospective diagnosis with MR imaging and explantation correlation. Radiology 2001;219:445–454.
98. Lim JH, Cho JM, Kim EY, et al. Dysplastic nodules in liver cirrhosis: Evaluation of hemodynamics with CT during arterial portography and CT hepatic arteriography. Radiology 2000;214:869–874.
99. Earls JP, Theise ND, Weinreb JC, et al. Dysplastic nodules and hepatocellular carcinoma: Thin-section MR imaging of explanted cirrhotic livers with pathologic correlation. Radiology 1996;201:207–214.
100. Matsui O, Kadoya M, Kameyama T, et al. Adenomatous hyperplastic nodules in the cirrhotic liver: Differentiation from hepatocellular carcinoma with MR imaging. Radiology 1989;173:123–126.
101. Edmonson HA, Steiner PE. Primary carcinoma of the liver: A study of 100 cases among 48900 necropsies. Cancer 1954;7:462–503.
102. Ishizaki M, Ashida K, Higashi T, et al. The formation of capsule and septum in human hepatocellular carcinoma. Virchows Arch 2001;438:574–580.
103. Tanaka M, Nakashima O, Wada Y, et al. Pathomorphological study of Kupffer cells in hepatocellular carcinoma and hyperplastic nodular lesions in the liver. Hepatology 1996;24:807–812.
104. Ebara M, Ohto M, Watanabe Y, et al. Diagnosis of small hepatocellular carcinoma: Correlation of MR imaging and tumor histologic studies. Radiology 1986;159:371–377.
105. Kadoya M, Matsui O, Takashima T, et al. Hepatocellular carcinoma: Correlation of MR imaging and histopathologic findings. Radiology 1992;183:819–825.
106. Yamashita Y, Fan ZM, Yamamoto H, et al. Spin-echo and dynamic gadolinium-enhanced FLASH MR imaging of hepatocellular carcinoma: Correlation with histopathologic findings. J Magn Reson Imaging 1994;4:83–90.
107. Winter TC 3rd, Takayasu K, Muramatsu Y, et al. Early advanced hepatocellular carcinoma: Evaluation of CT and MR appearance with pathologic correlation. Radiology 1994;192:379–387.
108. Ebara M, Fukuda H, Kojima Y, et al. Small hepatocellular carcinoma: Relationship of signal intensity to histopathologic findings and metal content of the tumor and surrounding hepatic parenchyma. Radiology 1999;210:81–88.
109. Marti-Bonmati L. MR imaging characteristics of hepatic tumors. Eur Radiol 1997;7:249–258.
110. Earls JP, Rofsky NM, DeCorato DR, et al. Hepatic arterial-phase dynamic gadolinium-enhanced MR imaging: Optimization with a test examination and a power injector. Radiology 1997;202:268–273.
111. Frederick MG, McElaney BL, Singer A, et al. Timing of parenchymal enhancement on dual-phase dynamic helical CT of the liver: How long does the hepatic arterial phase predominate? AJR Am J Roentgenol 1996;166:1305–1310.
112. Yu JS, Kim KW, Kim EK, et al. Contrast enhancement of small hepatocellular carcinoma: Usefulness of three successive early image acquisitions during multiphase dynamic MR imaging. AJR Am J Roentgenol 1999;173:597–604.
113. Grazioli L, Olivetti L, Fugazzola C, et al. The pseudocapsule in hepatocellular carcinoma: Correlation between dynamic MR imaging and pathology. Eur Radiol 1999;9:62–67.
114. Grazioli L, Morana G, Caudana R, et al. Hepatocellular carcinoma: Correlation between gadobenate dimeglumine-enhanced MRI and pathologic findings. Invest Radiol 2000;35:25–34.
115. Grazioli L, Morana G, Schneider G, et al. Hypervascular hepatic lesions: Dynamic and late enhancement pattern with Gd-BOPTA. In: RSNA; 2001. Chicago: Radiology, 2001;105. AU10
116. Kane PA, Ayton V, Walters HL, et al. MnDPDP-enhanced MR imaging of the liver. Correlation with surgical findings. Acta Radiol 1997;38(4 pt 2):650–654.
117. Ni Y, Marchal G, Yu J, et al. Experimental liver cancers: Mn-DPDP-enhanced rims in MR-microangiographic-histologic correlation study. Radiology 1993;188:45–51.
118. Helmberger TK, Laubenberger J, Rummeny E, et al. MRI characteristics in focal hepatic disease before and after administration of MnDPDP: Discriminant analysis as a diagnostic tool. Eur Radiol 2002;12:62–70.
119. Lim JH, Choi D, Cho SK, et al. Conspicuity of hepatocellular nodular lesions in cirrhotic livers at ferumoxides-enhanced MR imaging: Importance of Kupffer cell number. Radiology 2001;220:669–676.
120. Tang Y, Yamashita Y, Arakawa A, et al. Detection of hepatocellular carcinoma arising in cirrhotic livers: Comparison of gadolinium- and ferumoxides-enhanced MR imaging. AJR Am J Roentgenol 1999;172:1547–1554.
121. Vogl TJ, Hammerstingl R, Schwarz W, et al. Superparamagnetic iron oxide–enhanced versus gadolinium-enhanced MR imaging for differential diagnosis of focal liver lesions. Radiology 1996;198:881–887.
122. Kubaska S, Sahani DV, Saini S, et al. Dual contrast enhanced magnetic resonance imaging of the liver with superparamagnetic

iron oxide followed by gadolinium for lesion detection and characterization. Clin Radiol 2001;56:410–415.
123. Ward J, Guthrie JA, Scott DJ, et al. Hepatocellular carcinoma in the cirrhotic liver: Double-contrast MR imaging for diagnosis. Radiology 2000;216:154–162.
124. Pauleit D, Textor J, Bachmann R, et al. Hepatocellular carcinoma: Detection with gadolinium- and ferumoxides-enhanced MR imaging of the liver. Radiology 2002;222:73–80.
125. Ichikawa T, Federle MP, Grazioli L, et al. Fibrolamellar hepatocellular carcinoma: Imaging and pathologic findings in 31 recent cases. Radiology 1999;213:352–361.
126. McLarney JK, Rucker PT, Bender GN, et al. Fibrolamellar carcinoma of the liver: Radiologic-pathologic correlation. Radiographics 1999;19:453–471.
127. Burkill GJ, Mannion EM, Healy JC. Technical report: Lymph node enhancement at MRI with MnDPDP in primary hepatic carcinoma. Clin Radiol 2001;56:67–71.
128. Hanafusa K, Ohashi I, Himeno Y, et al. Hepatic hemangioma: Findings with two-phase CT. Radiology 1995;196:465–469.
129. van Leeuwen MS, Noordzij J, Feldberg MA, et al. Focal liver lesions: Characterization with triphasic spiral CT. Radiology 1996; 201:327–336.
130. Kim T, Federle MP, Baron RL, et al. Discrimination of small hepatic hemangiomas from hypervascular malignant tumors smaller than 3 cm with three-phase helical CT. Radiology 2001; 219:699–706.
131. Vilgrain V, Boulos L, Vullierme MP, et al. Imaging of atypical hemangiomas of the liver with pathologic correlation. Radiographics 2000;20:379–397.
132. Semelka RC, Cumming MJ, Shoenut JP, et al. Islet cell tumors: Comparison of dynamic contrast-enhanced CT and MR imaging with dynamic gadolinium enhancement and fat suppression. Radiology 1993;186:799–802.
133. Larson RE, Semelka RC, Bagley AS, et al. Hypervascular malignant liver lesions: Comparison of various MR imaging pulse sequences and dynamic CT. Radiology 1994;192:393–399.
134. Mahfouz AE, Hamm B, Wolf KJ. Peripheral washout: A sign of malignancy on dynamic gadolinium-enhanced MR images of focal liver lesions. Radiology 1994;190:49–52.
135. Ferrucci JT. Liver tumor imaging. Current concepts. Radiol Clin North Am 1994;32:39–54.
136. Fong Y, Blumgart LH, Fortner JG, et al. Pancreatic or liver resection for malignancy is safe and effective for the elderly. Ann Surg 1995;222:426–434, discussion 434–427.
137. Wernecke K, Rummeny E, Bongartz G, et al. Detection of hepatic masses in patients with carcinoma: Comparative sensitivities of sonography, CT, and MR imaging. AJR Am J Roentgenol 1991; 157:731–739.
138. Schulz W, Borchard F. The size of the liver metastases in a low metastatic count. A quantitative study of postmortem livers. Rofo Fortschr Geb Rontgenstr Neuen Bildgeb Verfahr 1992;156:320–324.
139. Semelka RC, Mitchell DG. Liver and biliary system. In: Edelman RR, Zlatkin MB, Hesselink JR, eds. Clinical Magnetic Resonance Imaging. Philadelphia: WB Saunders, 1996;1466–1512.
140. Semelka RC, Kelekis NL. Liver. In: Semelka RC, Ascher SM, Reinhold C, eds. MRI of the Abdomen and Pelvis. New York: Wiley-Liss, 1997;19–135.
141. Semelka RC, Helmberger TK. Contrast agents for MR imaging of the liver. Radiology 2001;218:27–38.
142. Outwater E, Tomaszewski JE, Daly JM, et al. Hepatic colorectal metastases: Correlation of MR imaging and pathologic appearance. Radiology 1991;180:327–332.
143. Semelka RC, Bagley AS, Brown ED, et al. Malignant lesions of the liver identified on T1- but not T2-weighted MR images at 1.5 T. J Magn Reson Imaging 1994;4:315–318.
144. Semelka RC, Cance WG, Marcos HB, et al. Liver metastases: Comparison of current MR techniques and spiral CT during arterial portography for detection in 20 surgically staged cases. Radiology 1999;213:86–91.
145. Reimer P, Rummeny EJ, Daldrup HE, et al. Enhancement characteristics of liver metastases, hepatocellular carcinomas, and hemangiomas with Gd-EOB-DTPA: Preliminary results with dynamic MR imaging. Eur Radiol 1997;7:275–280.
146. Ward J, Naik KS, Guthrie JA, et al. Hepatic lesion detection: Comparison of MR imaging after the administration of superparamagnetic iron oxide with dual-phase CT by using alternative-free response receiver operating characteristic analysis. Radiology 1999; 210:459–466.
147. Oudkerk M, van den Heuvel AG, Wielopolski PA, et al. Hepatic lesions: Detection with ferumoxide-enhanced T1-weighted MR imaging. Radiology 1997;203:449–456.
148. Semelka RC, Lee JK, Worawattanakul S, et al. Sequential use of ferumoxide particles and gadolinium chelate for the evaluation of focal liver lesions on MRI. J Magn Reson Imaging 1998;8:670–674.
149. Ward J, Robinson PJ. Combined use of MR contrast agents for evaluating liver disease. Magn Reson Imaging Clin N Am 2001; 9:767–802, vi.
150. van Gansbeke D, Metens TM, Matos C, et al. Effects of AMI-25 on liver vessels and tumors on T1-weighted turbo-field-echo images: Implications for tumor characterization. J Magn Reson Imaging 1997;7:482–489.
151. Ros PR. Benign liver lesion. In: Gore RM, Levin MS, Laufer I, eds. Textbook of Gastrointestinal Radiology. Philadelphia: WB Saunders, 1994:1861–1896.
152. Reddy KR, Kligerman S, Levi J, et al. Benign and solid tumors of the liver: Relationship to sex, age, size of tumors, and outcome. Am Surg 2001;67:173–178.
153. Valls C, Rene M, Gil M, et al. Giant cavernous hemangioma of the liver: Atypical CT and MR findings. Eur Radiol 1996;6:448–450.
154. Mergo PJ, Ros PR. Benign lesions of the liver. Radiol Clin North Am 1998;36:319–331.
155. Weimann A, Ringe B, Klempnauer J, et al. Benign liver tumors: Differential diagnosis and indications for surgery. World J Surg 1997;21:983–990, discussion 990–981.
156. Semelka RC, Brown ED, Ascher SM, et al. Hepatic hemangiomas: A multi-institutional study of appearance on T2-weighted and serial gadolinium-enhanced gradient-echo MR images. Radiology 1994;192:401–406.
157. Soyer P, Gueye C, Somveille E, et al. MR diagnosis of hepatic metastases from neuroendocrine tumors versus hemangiomas: Relative merits of dynamic gadolinium chelate-enhanced gradient-recalled echo and unenhanced spin-echo images. AJR Am J Roentgenol 1995;165:1407–1413.
158. Yu JS, Kim MJ, Kim KW, et al. Hepatic cavernous hemangioma: Sonographic patterns and speed of contrast enhancement on multiphase dynamic MR imaging. AJR Am J Roentgenol 1998;171: 1021–1025.
159. Whitney WS, Herfkens RJ, Jeffrey RB, et al. Dynamic breath-hold multiplanar spoiled gradient-recalled MR imaging with gadolinium enhancement for differentiating hepatic hemangiomas from malignancies at 1.5 T. Radiology 1993;189:863–870.
160. Bloom CM, Langer B, Wilson SR. Role of US in the detection, characterization, and staging of cholangiocarcinoma. Radiographics 1999;19:1199–1218.
161. Sherlock S, Dooley J. Disease of the Liver and Biliary System. London: Blackwell, 1997.
162. Fernandez MP, Redvanly RD. Primary hepatic malignant neoplasms. Radiol Clin North Am 1998;36:333–348.
163. Hashimoto T, Nakamura H, Hori S, et al. MR imaging of mixed hepatocellular and cholangiocellular carcinoma. Abdom Imaging 1994;19:430–432.
164. Vilgrain V, Van Beers BE, Flejou JF, et al. Intrahepatic cholan-

giocarcinoma: MRI and pathologic correlation in 14 patients. J Comput Assist Tomogr 1997;21:59–65.
165. Klempnauer J, Ridder GJ, Werner M, et al. What constitutes long-term survival after surgery for hilar cholangiocarcinoma? Cancer 1997;79:26–34.
166. Okuda K, Kubo Y, Okazaki N, et al. Clinical aspects of intrahepatic bile duct carcinoma including hilar carcinoma: A study of 57 autopsy-proven cases. Cancer 1977;39:232–246.
167. Maetani Y, Itoh K, Watanabe C, et al. MR imaging of intrahepatic cholangiocarcinoma with pathologic correlation. AJR Am J Roentgenol 2001;176:1499–1507.
168. Murakami T, Nakamura H, Tsuda K, et al. Contrast-enhanced MR imaging of intrahepatic cholangiocarcinoma: Pathologic correlation study. J Magn Reson Imaging 1995;5:165–170.
169. Zhang Y, Uchida M, Abe T, et al. Intrahepatic peripheral cholangiocarcinoma: Comparison of dynamic CT and dynamic MRI. J Comput Assist Tomogr 1999;23:670–677.
170. Yoshida Y, Imai Y, Murakami T, et al. Intrahepatic cholangiocarcinoma with marked hypervascularity. Abdom Imaging 1999;24:66–68.
171. Vogl TJ, Hammerstingl R, Schwarz W, et al. Magnetic resonance imaging of focal liver lesions. Comparison of the superparamagnetic iron oxide Resovist versus gadolinium-DTPA in the same patient. Invest Radiol 1996;31:696–708.